Geochimica et Cosmochimica Acta 371 (2024) 126–143

Contents lists available at ScienceDirect

Geochimica et Cosmochimica Acta

journal homepage: www.elsevier.com/locate/gca

Redox cycling of straw-amended soil simultaneously increases iron oxide crystallinity and the content of highly disordered organo-iron(III) solids

Christian Mikutta [a,*], Max Niegisch [a], Aaron Thompson [b], Ricarda Behrens [a], Laura S. Schnee [a], Martin Hoppe [c], Reiner Dohrmann [c,d]

[a] Soil Mineralogy, Institute of Mineralogy, Gottfried Wilhelm Leibniz University Hannover, Callinstr. 3, D-30167 Hannover, Germany
[b] Crop and Soil Sciences, University of Georgia, Athens, GA 30602-7272, United States
[c] Federal Institute for Geosciences and Natural Resources (BGR), Stilleweg 2, D-30655 Hannover, Germany
[d] State Authority of Mining, Energy and Geology (LBEG), Stilleweg 2, D-30655 Hannover, Germany

ARTICLE INFO

Associate editor: Elizabeth Herndon

Keywords:
Soil
Iron speciation
Redox fluctuations
Reduction and oxidation
Organic matter
Straw amendment
Selective extractions
X-ray absorption spectroscopy
Mössbauer spectroscopy

ABSTRACT

Iron speciation in soils is influenced largely by its redox state, but the extent of and controls on Fe speciation during recurrent reduction and oxidation events are not fully understood. To investigate the effects of organic matter (OM) inputs and the frequency and duration of redox oscillations on soil Fe speciation, we conducted redox-oscillation experiments with topsoil from a Fluvisol mixed with rice straw (0, 10, 50 g/kg organic carbon, OC). The soil was initially dominated by short-range ordered (SRO) Fe(III) solids and subjected to 14- and 28-day reduction–oxidation cycles for 112 days, with the time spent under anoxic and oxic conditions maintained at 6:1. Reduction was initiated by flooding reactors with artificial river water. To simulate leaching conditions, soil re-oxidation was achieved by air-drying soil after removal of reacted solutions. Fresh river water was then added for each new redox cycle. We monitored changes in solution composition (E_h, pH, Fe(II), total Fe, OC, and Si) and assessed changes of solid-phase Fe speciation by selective extractions, X-ray absorption spectroscopy, and ^{57}Fe Mössbauer spectroscopy. Dissolved OC and Fe increased with increasing straw addition, but decreased in each treatment through consecutive reduction intervals. Release rates of dissolved Fe and OC were highly correlated, implying that microbial reduction of soil Fe(III) solids was fostered by straw amendments. Reduction-induced losses of OC and Fe from straw amended soil were amplified at high redox frequency. Ferrous Fe did not detectably accumulate in the solid phase upon repeated soil oxidation. Although Fe(III)-poor phyllosilicates gained in relative importance in redox-cycled soils, their fraction was hardly affected during redox cycling. Instead, straw additions led to an enhanced depletion of ferrihydrite during soil redox cycling and a relative enrichment of highly disordered Fe(III) species ['very SRO (vSRO) Fe(III) solids'], which remained only partially ordered in 5-K Mössbauer spectra and likely consisted predominantly of polynuclear organic Fe complexes. The depletion of ferrihydrite in straw-amended soils after 112 days was greater in the 14-day cycle than in the 28-day cycle experiment and accompanied by a less pronounced enrichment of vSRO Fe(III) solids. The crystallinity of distinct Fe oxides (ferrihydrite, lepidocrocite, and hematite) increased during soil redox cycling especially in straw-amended soils, but without noticeable ferrihydrite conversion into crystalline Fe oxides. The increase in the crystallinity of distinct Fe oxides after 112 days was greater at low redox frequency in straw-free soil, however this frequency effect was suppressed by straw additions. Longer soil redox cycling (112 vs. 56 days) increased the crystallinity of distinct Fe oxides, which was most pronounced at high straw levels and low redox frequency. Our results imply that redox changes in SRO Fe oxide- and OM-rich soils can cause a relative enrichment of more crystalline Fe oxides, while still maintaining a pool of vSRO Fe(III) solids. We conclude that soil redox oscillations can lead to divergent transformation pathways of Fe oxides, which concomitantly increase bulk Fe-oxide crystallinity and generate increasing fractions of highly disordered Fe(III) solids on comparatively short time scales. In addition, our study suggests that faster redox cycling in soils with ample electron donor supply and water leaching leads to higher element exports (e.g., OC, metal(loid)s) from soil due to weekly redox pulsing than more slowly alternating redox conditions.

* Corresponding author.
E-mail address: c.mikutta@mineralogie.uni-hannover.de (C. Mikutta).

https://doi.org/10.1016/j.gca.2024.02.009
Received 17 July 2023; Accepted 15 February 2024
Available online 22 February 2024

1. Introduction

Dynamic redox conditions are a major determinant of microbial activity and mineral reactivity in soils (Lacroix et al., 2023). In wetland and upland soils, redox conditions can change on a daily, weekly or seasonal basis due to shifting moisture contents and water-table levels (Barcellos et al., 2018). The temporal dynamics of hydrologic flow conditions can create steep soil redox gradients influencing mineral (trans)formation reactions and mineral reactivity towards major and trace elements (Zhang and Furman, 2021).

In water-saturated soils, any O_2 initially present is rapidly consumed by microbial respiration. Since O_2 supply is strongly limited when pores are filled with water, anoxic conditions establish and alternative electron acceptors such as nitrate, Mn(III/IV) and Fe(III) (oxyhydr)oxides (hereafter collectively termed oxides), and sulfate are subsequently used for microbial respiration instead of O_2 (Reddy and DeLaune, 2008). The sequence of alternative electron acceptors generally follows thermodynamic yield, beginning with nitrate. Once nitrate is consumed, reductive dissolution of Mn- and Fe oxides ensues, increasing dissolved Mn(II) and Fe(II) concentrations up to millimolar levels, which can trigger the release of Na, K, Ca, and Mg into the soil solution following cation exchange. Concurrently, dissolved carbonate concentrations increase due to microbial respiration. Reductive proton consumption and carbonate production buffer soil pH to slightly acidic to neutral values during soil inundation (Kirk, 2004). At a later stage of submergence, sulfate is used as electron acceptor, resulting in the formation of hydrogen sulfide (HS^-). These major anoxia-induced changes in soil chemistry profoundly affect the presence and stability of solid Fe phases. High solution concentrations of Fe(II) can promote the recrystallization or transformation of existing Fe oxides into new phases (Fredrickson et al., 1998; Hansel et al., 2003; Mejia et al., 2016; Tomaszewski et al., 2016; Zachara et al., 2002). Prominent examples of newly formed Fe phases include green rust ($[Fe^{II}_{6-x}Fe^{III}_x(OH)_{12}][A^{2-}]_{x/2}\cdot nH_2O$) (Abdelmoula et al., 1998; Trolard et al., 1997), magnetite (Fe_3O_4) (Maher and Taylor, 1988; Vandenberghe et al., 1998), and Fe sulfides such as mackinawite (FeS), greigite (Fe_3S_4), and pyrite (FeS_2) (Burton et al., 2011; Langner et al., 2012). Upon soil re-aeration, rapid oxidation of dissolved Fe(II) in presence of high dissolved organic carbon (DOC) or Si concentrations can lead to the formation of short range-ordered (SRO) Fe oxides, notably ferrihydrite ($\sim Fe_5HO_8\cdot 4H_2O$) (Chen and Thompson, 2018; Cornell and Schwertmann, 2003). The oxidation of Fe sulfides can generate substantial amounts of acidity and thereby decrease soil pH as shown for acid sulfate soils and sites affected by acid mine drainage (Blowes et al., 2003; Burton et al., 2011).

The general changes in chemistry and mineral composition upon either soil reduction or oxidation have been well studied in the past, but there is less information available on how repeated fluctuations in soil redox conditions impact soil Fe speciation. This aspect has been addressed by several field studies. Studies on Alisol, Andosol, and Vertisol paddy soils revealed that seasonal wetting and drying for centuries can result in high Fe losses in topsoils and that the crystallinity of Fe oxides depends on their initial assemblage (crystalline vs. SRO minerals) and water leaching rate. High leaching rates tend to enrich crystalline and low leaching rates SRO Fe oxides (Winkler et al., 2018, 2016). Similar results were obtained by Vogelsang et al., (2016b) for a chronosequence of 0.1, 0.7, and 2 ka-old paddy soils. Prolonged paddy cultivation resulted in a general loss of oxide-bound Fe in topsoils and the remaining Fe-oxide assemblage became progressively dominated by organic C (OC)-rich SRO Fe phases. In contrast, the total amount of Fe oxides in the subsoils increased owing to precipitation of Fe leached from topsoils. Micro-crystalline goethite (α-FeOOH) was the predominating Fe-oxide phase in the upper subsoil, likely due to Fe(II)-catalyzed solid-state transformation of freshly precipitated ferrihydrite (Vogelsang et al., 2016b). The long-term accumulation of SRO Fe oxides has also been reported for other paddy soils (Huang et al., 2020).

Studies targeting the effect of redox fluctuations on Fe speciation in non-paddy soils are rare. Thompson et al. (2011) investigated changes in soil Fe concentration and its solid-phase speciation across a 400 ka-old basaltic lava flow subjected to a gradient in precipitation (2200–4200 mm/a) and redox dynamics. With increasing rainfall and decreasing redox potential (E_h), total Fe decreased from about 25 % to < 1 % of soil mass. The Fe-oxide fraction of total Fe decreased with increasing rainfall and was replaced by a corresponding increase in the organic/silicate Fe fraction. In addition, the crystallinity of the Fe oxides decreased with increasing rainfall and leaching, with the most disordered members of the crystallinity continuum, the nano-Fe oxides, gaining proportional importance at wetter sites. Barcellos et al. (2018) reported for Puerto Rican rain forest soils (Inceptisols, Oxisols, and Ultisols) that day-to-week rainfall fluctuations are accompanied by changes in rapidly reducible Fe oxides, constituting 42 to 100 % of the soil SRO Fe oxide pool. In contrast, Mansfeldt et al. (2012) showed that lasting water saturation and frequent anoxic conditions led to an enrichment of goethite rather than ferrihydrite in a Haplic Gleysol developed from Holocene fluvial loam overlaying glaciofluvial sand, which they ascribed to the better availability of ferrihydrite for microbial Fe reduction.

Apart from field studies, several laboratory studies have examined changes in soil Fe speciation during oscillating redox conditions. In a benchmark study, Thompson et al. (2006) conducted a redox-stat reactor experiment in which an Inceptisol A-horizon was subjected to a series of four reduction–oxidation cycles, each lasting 14 days. The initial soil contained large amounts of SRO minerals such as nanogoethite and allophane $[(Al_2O_3)(SiO_2)_{1.3-2.0}(H_2O)_{2.5-3.0}]$, but no detectable ferrihydrite. The cumulative response of soil solids during multiple redox oscillations showed (1) a decrease in SRO Fe phases and (2) a transformation of nano- into micro-crystalline goethite and hematite (α-Fe_2O_3), demonstrating that short-term redox oscillations can increase the crystallinity of soil Fe oxides. This result could not be confirmed by Parsons et al. (2013), who found little variation in Fe speciation in As-spiked A horizon material of a Mollic Fluvisol after 77 days of redox cycling with 7-day intervals of oxidizing and reducing conditions. Their result was explained by the high frequency of redox oscillations and therefore limited extent of Fe reduction and oxidation when compared to the total Fe pool (Parsons et al., 2013). Similarly, Ginn et al. (2017) examined the influence of temporal O_2 variations on Fe speciation in Ultisols from the Luquillo Critical Zone Observatory (Puerto Rico). Soil slurries were exposed to alternating oxic-anoxic conditions at redox frequencies of 3.5, 7, and 14 days/cycle at constant pH with and without phosphate addition for up to 56 days. The ratio of time under anoxic/oxic conditions (t_{anoxic}:t_{oxic}) was maintained at 6:1 in all treatments. Their results showed increasing rates of soil Fe(II) production over the experimental duration with a concomitant increase of an Fe(II) concentration plateau within each anoxic period. Modeling suggested that Fe(II) dynamics can be explained by the formation of rapidly reducible SRO Fe phases derived from the progressive dissolution of native Fe oxides and re-oxidation of Fe(II). The shift in Fe reactivity was evidenced by Fe-reducibility assays using *Shewanella* sp., but remained undetectable by chemical extractions and spectroscopic analyses, most likely due to minor changes in Fe speciation in relation to the soil Fe pool. A series of studies using ^{57}Fe isotope labelling indeed showed that recently precipitated Fe oxides increased the availability of Fe towards microbial reduction, but also that their speciation depends strongly on oxidation rate and the presence of Fe oxides and organic matter (OM) (Chen et al., 2020, 2018; Chen and Thompson, 2021, 2018). Similarly, Bhattacharyya et al. (2018) incubated material of a Puerto Rican forest soil (clayey Oxisol) in closed reactors under varying redox conditions for 44 days. The material was subjected to redox cycles at frequencies of 12 and 8 days/cycle with the ratios of days spent under oxic and anoxic conditions per cycle of 8:4 and 4:4, respectively. After 44 days, no differences in Fe speciation could be detected using selective extractions and X-ray absorption spectroscopy (XAS), whereas samples incubated under constant anoxic conditions showed complete

dissolution of goethite and an enrichment in ferrihydrite and pyrite.

Despite documented efforts to decipher Fe speciation changes in soils under redox-dynamic conditions, previous results are hard to generalize. This is because some studies illustrated that Fe-oxide crystallinity can increase (Thompson et al., 2006; Vogelsang et al., 2016a), decrease (Mansfeldt et al., 2012; Thompson et al., 2011; Vogelsang et al., 2016b; Winkler et al., 2016), or that crystallinity changes remain largely undetectable (Ginn et al., 2017; Parsons et al., 2013) during redox fluctuations. These contrasting findings likely originate from different environmental conditions, as the composition of Fe(III) solids in redox-active soils depends in complex ways on O_2 fugacity, mineralogy, OM content, and soil moisture regime (Barcellos et al., 2018; Chen et al., 2020, 2018; Chen and Thompson, 2021, 2018; Winkler et al., 2018, 2016). One may also speculate that conflicting findings are at least in part related to experimental design. Some authors investigated redox-driven changes in Fe mineral composition under completely water-saturated conditions in closed reactors, often with agitation of soil suspensions (Ginn et al., 2017; Parsons et al., 2013; Thompson et al., 2006) or at a constant moisture content (Bhattacharyya et al., 2018). Others explored natural soil systems subjected to repeated wetting and drying cycles over extended periods of time during which soil water was allowed to drain freely, resulting in partial removal of reduced solution species such as Fe(II) under anoxic conditions (Mansfeldt et al., 2012; Thompson et al., 2011; Vogelsang et al., 2016b, 2016a; Winkler et al., 2018, 2016). Besides the uncertainty related to the effect of different water regimes ('leaching' vs. 'non-leaching' conditions), the effect of redox frequency on Fe species (trans)formations during soil redox oscillations has rarely been addressed (Bhattacharyya et al., 2018; Ginn et al., 2017). These studies showed little effects on bulk Fe speciation, most likely due to the high redox frequency (≤14 days/redox cycle). Furthermore, the impact of OM on Fe speciation changes during soil redox fluctuations remains elusive. The increase in soil pH during anoxia drives the solubilization of OM (Grybos et al., 2009), and DOC formed may interfere with dissimilatory Fe mineral reduction and transformation reactions (Braunschweig et al., 2014; Piepenbrock et al., 2011) with hitherto unclear consequences for soil Fe pools.

The objective of this study was to clarify whether (1) OM promotes the formation of SRO Fe(III) species during soil redox oscillations, (2) redox frequency affects solid-phase Fe speciation, and (3) sustained redox cycling of soil under leaching conditions causes the accumulation of SRO Fe oxides. Therefore, we conducted 112-day incubation experiments with soil mixed with different amounts of rice straw as a cellulose-rich OC source for soil microorganisms. We varied the frequency of oxidation–reduction cycles and monitored Fe speciation changes in the liquid- and solid phase. The experiments also allowed us to test for the effect of redox fluctuation time (i.e., the number of reduction–oxidation cycles) on soil Fe speciation. Since adsorbed or coprecipitated OM impairs reduction and recrystallization of SRO Fe oxides under reducing conditions (Chen et al., 2015; Eusterhues et al., 2014), we hypothesized that increasing OM levels lead to increased proportions of Fe associated with SRO Fe oxides during soil redox cycling. Additionally, we hypothesized that a lower redox frequency results in greater changes of soil Fe pools due to longer anoxia and that speciation changes become more pronounced with increasing redox fluctuation time.

2. Materials and methods

Topsoil material of a Gleyic Fluvisol (0–15 cm depth, grassland) was sampled from the Mulde river floodplain near Muldenstein (51°39′24.8″ N, 12°19′48.4″ E), Saxony-Anhalt, Germany, air-dried, sieved to < 2 mm particle size, and manually removed of visible plant remains. The soil was then stored at room temperature in the dark. Rice straw (*Oryza sativa*) was sourced from the Rice Research Centre (Ente Nazionale Risi) of Pavia, Italy, and crushed into fibrous fragments < 5 mm. All reagents and standards were of analytical grade or higher. Experimental solutions were always prepared with ultrapure water (resistivity ≥ 18.2 MΩ cm). Materials transferred into a glovebox were equilibrated in the antechamber overnight to remove traces of O_2.

2.1. Soil and rice-straw characterization

Soil pH was measured in 0.01 M $CaCl_2$ (1:5 v/v; DIN EN ISO 10390) using a SenTix® 51 electrode (WTW). Total C (C_{tot}) and N (N_{tot}) were analyzed in triplicates by dry catalytic high-temperature combustion using a vario MAX cube elemental analyzer (Elementar Analysensysteme GmbH). Particle size distribution of the silicate fine earth was determined in triplicates by sieving and sedimentation (ISO 11277). Effective cation exchange capacity (ECEC) and base saturation (BS) were determined in triplicates using an unbuffered 0.1 M $BaCl_2$ solution according to DIN EN ISO 11260. In this method, $BaCl_2$-saturated soils are additionally treated with a 0.02 M $MgSO_4$ solution (compulsive exchange) to determine the ECEC by Mg occupancy on exchangeable cation sites (Gillman, 1979). Exchangeable Al, Ca, Fe, K, Mn, Na, and Mg were determined by inductively coupled plasma–optical emission spectrometry (ICP-OES, Agilent 5900 SVDV). ECEC ($cmol_c/kg$) was calculated from exchangeable cations excluding protons following Hendershot et al., (2008a). Base saturation (%) was calculated as $\sum(Na + K + Ca + Mg)$ / ECEC × 100 and exchangeable acidity (EA) was assessed by titration of the $BaCl_2$-centrifugates with 0.02 M NaOH (Hendershot et al., 2008a, 2008b). Dithionite-citrate-bicarbonate- and acid ammonium oxalate-extractable Fe (Fe_d and Fe_o, respectively) were determined in triplicates based on Mehra and Jackson (1958) and Schwertmann (1964). Iron concentrations were measured in solutions obtained after centrifugation (Fe_d: 15 min at 4000 × *g*, Fe_o: 15 min at 3000 × *g*) using ICP-OES (PQ 9000 Elite, Analytik Jena). Total element contents were determined by wavelength-dispersive X-ray fluorescence (XRF) spectrometry analysis of fused glass beads employing a PANalytical Axios instrument. To determine loss on ignition, 1.000 g of sample material was heated to 1030 °C for 10 min. After mixing the residue with 5.0 g lithium metaborate and 25 mg lithium bromide, samples were fused at 1200 °C for 20 min. Instrument calibrations were validated by analysis of reference materials, and in-house standards as well as 130 certified reference materials were used for correction procedures. Table 1 details the soil and rice-straw characteristics.

2.2. Redox experiments

All experiments were conducted in triplicates in the dark at 21 ± 2 °C. Three hundred grams of live soil were placed in Al foil-wrapped 1-L polypropylene (PP) centrifuge bottles and mixed with rice straw to achieve straw levels of 10 g/kg OC ('low-OC') and 50 g/kg OC ('high-OC'), which are in the range of studies on the effect of crop residues on soil OC dynamics (Duong et al., 2009; Pei et al., 2015; Su et al., 2020). Straw-free soil ('control') and soil-straw mixtures were suspended in 0.6 L of anoxic artificial river water (0.6 mM $CaSO_4$, 0.3 mM $Mg(NO_3)_2$, 0.6 mM NaCl) corresponding to the water composition of the Mulde river during the spring 1998 flood (Brandt, 2003). The capped bottles were transferred into an anoxic glovebox (N_2, 5.0 purity). Soils were not agitated between sampling during reduction periods to avoid disturbances of microbial communities (Dannenberg et al., 1997). The experiments were performed at redox frequencies (f_{redox}) of 14 and 28 days/cycle for a total duration of 112 days. The ratio of time spent under anoxic/oxic conditions (t_{anoxic}:t_{oxic}) was maintained at 6:1 in all treatments, that is, f_{redox} of 14 days/cycle resulted in 12 days of anoxic and 2 days of oxic conditions, and f_{redox} of 28 days/cycle in 24 days of anoxic and 4 days of oxic conditions. The frequencies chosen were based on typical inundation periods of floodplain soils in Central Europe (Kaden et al., 2021; Rolf et al., 2022), but are also relevant for upland soils receiving high-frequency precipitation (Barcellos et al., 2018). The soils underwent a total of eight redox cycles in the 14-day cycle experiment and four redox cycles in the 28-day cycle experiment. During reduction periods, the bottles were periodically opened to release CO_2

Table 1
Properties of the original soil and rice straw.[a]

Sand (wt%)	Silt (wt%)	Clay (wt%)	pH ($CaCl_2$)	ECEC ($cmol_c/kg$)	BS (%)	C (g/kg)	N (g/kg)	C/N (-)	P (g/kg)	Si (g/kg)	Fe_{tot} (g/kg)	Fe_d (g/kg)	Fe_o (g/kg)	Fe_o/Fe_d (-)	Fe_p (g/kg)
Soil															
26	51	23	5.7	22.2	99	54.4	4.3	12.6	4.4	278	35.7	17.4	10.2	0.59	3.8
Rice straw															
–	–	–	–	–	–	356	6.9	51.8	0.71	82.7	3.5	–	–	–	–

[a] Element contents and ECEC are given on a dry-weight basis. ECEC = effective cation exchange capacity. BS = base saturation. Fe_{tot} = total soil Fe content. Fe_d = dithionite-citrate-bicarbonate-extractable Fe. Fe_o = acid ammonium oxalate-extractable Fe. Fe_p = pyrophosphate-extractable Fe. '–' = not applicable or not analyzed.

pressure, record E_h and pH, and to retrieve ca. 10-mL suspension aliquots for solution analyses. The aliquots were centrifuged at 4700 × *g* for 20 min (closed tubes) and returned to the glovebox, where supernatants were passed through 0.2-µm Nylon membranes. The filtrates were transferred out of the glovebox, immediately acidified, and stored at ~ 5 °C for further analysis.

After each reduction period, closed soil bottles were transferred out of the glovebox and centrifuged at 3000 × *g* and 20 °C for 20 min. One part of the supernatant solutions was analyzed and treated for further analysis inside the glovebox as described above. Another part was transferred to 0.5-L PP bottles inside the glovebox, centrifuged again at 11000 × *g* for 20 min at 20 °C outside the glovebox, and then rapidly filtered through Whatman® glass fiber filters (0.7-µm pore size) to remove straw particles. The clear filtrates were covered with perforated Parafilm® and oxidized in ambient air at 21 °C for 48 h in the dark, analyzed for E_h and pH, and filtered through 0.2-µm Nylon membranes, acidified, and kept at ~ 5 °C for subsequent analysis.

Centrifuged soil of triplicate bottles was combined and spread out in covered plastic boxes for air-drying at 21 °C. Preliminary tests showed that soil centrifugation caused a negligible loss of clay (~1 wt% of the silicate fine earth). At the end of re-oxidation periods, air-dried soils were homogenized and divided among three bottles without mass loss, thereby reducing within-treatment variability. Artificial river water was again added to each bottle and the reduction-oxidation cycle repeated. The soil-to-solution ratio was always maintained at 1:2 (w/v) based on water content determinations of soil dried at 105 °C for 8 h. For each redox experiment, additional bottles were carried for solid-phase analyses, which were treated analogously. At the end of each oxic period, the solids were shock-frozen in liquid N_2 and freeze-dried. Fig. 1 shows the general experimental procedure including the targeted analytical parameters (see sections 2.3 and 2.4).

2.3. Solution analyses

During soil incubations, soil solutions were continuously monitored for E_h, pH, dissolved Fe(II) ($Fe(II)_{aq}$), total dissolved Fe (Fe_{aq}), dissolved Si, and DOC. Redox potential and pH were recorded with gel electrodes (SenTix® PtR and RJD, WTW) to minimize the efflux of K^+ and Cl^- into samples. Ferrous Fe concentrations were determined in acidified filtrates (10–50 vol% 0.5 M HCl Suprapur®) by the Ferrozine method

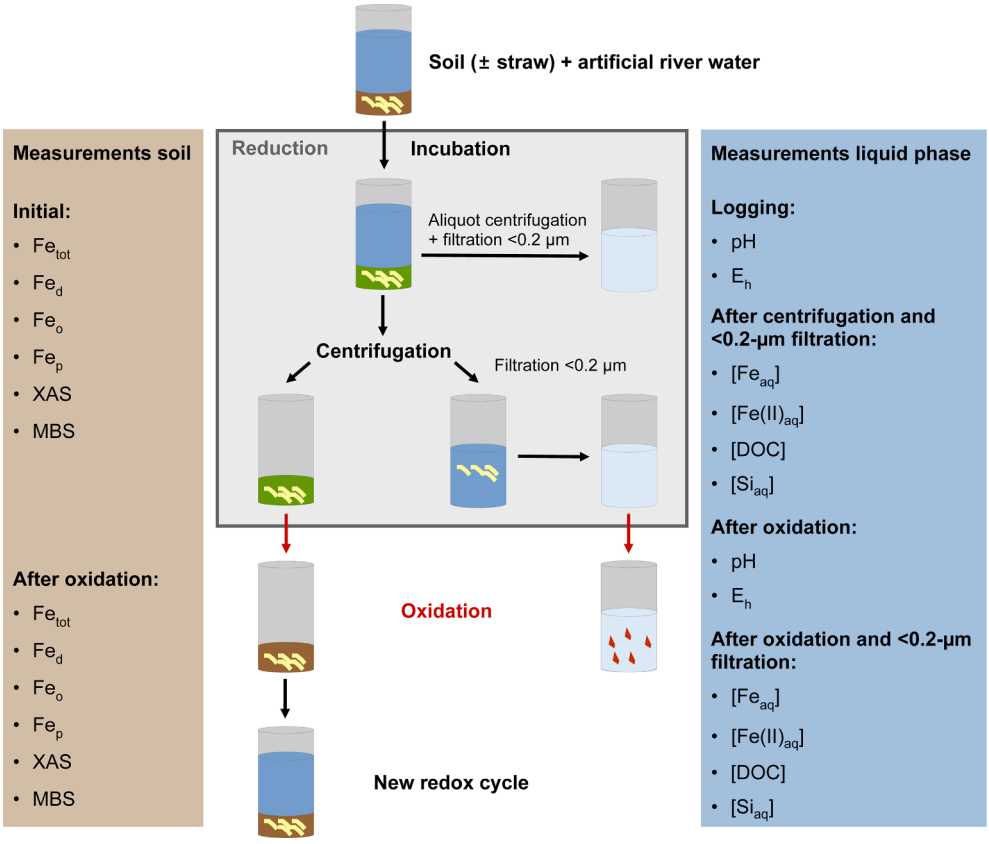

Fig. 1. Sampling scheme of the redox-oscillation experiments with information on analytical parameters and spectroscopies applied. Abbreviations: Fe_{tot} = total soil Fe content, Fe_d = dithionite-citrate-bicarbonate-extractable Fe, Fe_o = acid ammonium oxalate-extractable Fe, Fe_p = pyrophosphate-extractable Fe, XAS = X-ray absorption spectroscopy, MBS = Mössbauer spectroscopy, pH = -log (H^+), E_h = redox potential, $[Fe_{aq}]$ = concentration of total dissolved Fe, $[Fe(II)_{aq}]$ = concentration of dissolved Fe(II), [DOC] = concentration of dissolved organic carbon, $[Si_{aq}]$ = concentration of dissolved Si.

(Stookey, 1970) using a Cary 60 spectrophotometer (Agilent). Concentrations of Fe_{aq} and Si were measured in acidified filtrates (3 vol% of 65 % HNO_3 Suprapur®) by ICP-OES. DOC was analyzed as non-purgeable OC in filtrates acidified to pH 2–3 with 5 mM H_3PO_4 using a vario TOC select instrument (Elementar Analysensysteme GmbH).

2.4. Solid-phase analyses

2.4.1. Total Fe analysis and selective Fe extractions

All re-oxidized soil samples were analyzed in triplicates for total Fe (Fe_{tot}) using XRF spectrometry. Selective Fe extractions were used to track changes in operationally defined soil Fe pools during redox oscillations. Therefore, re-oxidized soil samples were analyzed in triplicates for Fe_d and Fe_o. Additionally, we determined pyrophosphate-soluble Fe (Fe_p) in triplicates following Mikutta et al. (2006). Soil was extracted at a soil-to-solution ratio of 1:100 (w/v) in 0.1 M $Na_4P_2O_7$ solution. The mixtures were shaken for 16 h and then a 50 mM $MgSO_4$ solution (1:10, v/v) was added to induce flocculation. The suspensions were centrifuged at 8200 × *g* for 10 min, filtered through 0.1-µm polyethersulfone membranes, and the filtrates analyzed for Fe by ICP-OES. Dithionite-citrate-bicarbonate extraction was used to quantify the sum of Fe bound in pedogenic Fe oxides and organic complexes, while acid ammonium oxalate extraction selectively removes Fe associated with SRO Fe oxides and organic complexes. Therefore, the Fe_o/Fe_d ratio is an approximation of the proportion of SRO Fe oxides in the total of all Fe oxides. Pyrophosphate is generally assumed to extract Fe largely from soil OM, even though it may also solubilize ferrihydrite or other nanometer-sized minerals to some extent (Rennert, 2019). The difference Fe_o–Fe_p can be taken as an estimate for SRO Fe oxides, primarily ferrihydrite (McKeague et al., 1971). For statistical analysis, all extraction parameters were expressed on an absolute dry weight basis (mg/kg soil) or relative to Fe_{tot} (e.g., Fe_d/Fe_{tot}, $(Fe_o–Fe_p)/Fe_{tot}$). Non-normalized values provide information on absolute gains or losses of specific Fe pools considering straw dilution factors, whereas normalized values indicate changes in Fe pools relative to Fe_{tot}.

2.4.2. X-ray absorption spectroscopy

To determine speciation changes of solid-phase Fe during soil redox cycling, the original soil and all re-oxidized soil samples of the high-frequency experiment (f_{redox} = 14 days/cycle) (N = 25) were analyzed as pressed 1.3-cm powder pellets by Fe K-edge (7112 eV) XAS at beamline 11.1 (XAFS) of the ELETTRA synchrotron facility (Trieste, Italy). The white beam was monochromatized with a Si(1 1 1) double-crystal monochromator, which was detuned by 40 % of the maximum intensity in order to reduce the higher harmonic content in the beam. Spectra were recorded at approximately 80 K in transmission mode using 30-cm Oxford Instruments™ ionization chambers. The monochromator was calibrated by setting the first inflection point in the K-edge absorption spectrum of a metallic Fe foil to 7112 eV. The foil was continuously measured to correct for slight energy offsets during sample measurements. The scans started at 6812 eV with a step size of 5 eV, which was reduced to 0.2 eV along the edge. The extended X-ray absorption fine structure (EXAFS) was recorded with a step size in *k*-space of 0.03 $Å^{-1}$. Three scans were collected per sample and averaged. Spectral data processing was performed in Athena (Ravel and Newville, 2005). The Autobk algorithm was applied for background removal using a linear pre-edge line between 200 and 50 eV before the edge, E_0, and a normalization range from 150 to 555 eV ($E–E_0$). The edge energy was defined as zero crossing of the second X-ray absorption near edge structure (XANES) derivative. By default, a quadratic polynomial was used as a post-edge line. The frequency cut-off parameter, R_{bkg}, was set to 0.9 and the *k*-weight in the background function determination to three. For quantification of Fe oxidation states and Fe species present, XANES and EXAFS spectra were evaluated by linear combination fitting (LCF) in Athena. XANES spectra were fit over −20 to 30 eV ($E–E_0$) and k^2-weighted EXAFS spectra over k = 2.0–11.0 $Å^{-1}$. For the latter, E_0 of all sample and reference spectra was set to 7130 eV. All reference spectra used in this study were taken from Langner et al. (2012) and Mikutta and Rothwell (2016).

2.4.3. Mössbauer spectroscopy

Transmission ^{57}Fe Mössbauer spectroscopy (MBS) was performed with a variable temperature He-cooled system with a 1024 channel detector at 295, 77, and 5 K. A ^{57}Co source (~50 mCi or less) embedded in a Rh matrix was used at room temperature. Freeze-dried powder samples of the original soil and re-oxidized soil samples obtained from both redox experiments after 56 and 112 days (N = 13) were mounted between two pieces of 0.127-mm thickness Kapton® tape and transferred to the spectrometer cryostat. Velocity (i.e., γ-ray energy) was calibrated using an α-Fe foil at 295 K and all center shifts (CSs) and peak positions are reported with respect to this standard. The transducer was operated in constant acceleration mode and folding was performed to achieve a flat background. Mössbauer spectral fitting of all spectra was performed using the Voigt-based fitting (VBF) method of Rancourt and Ping (1991) for quadrupole splitting distributions (QSDs) and combined hyperfine field distributions (HFDs), as implemented in the Recoil™ software (ISA Inc.). All VBF MB parameter definitions and a description of the relevant notation are given by Rancourt and Ping (1991). All errors in MB fitting parameters are two-standard deviation (2σ) errors, as calculated by Recoil™. In reporting quantitative phase abundances or site populations, we assumed that the MB recoilless fractions of all detected phases or Fe-bearing components are equal, so that subspectral areas, expressed as fractions of total spectral area, are equal to the amounts of Fe, expressed as fractions of Fe_{tot}, in the corresponding phases or components. Details of our MB fit approach can be found in Table S7.

2.5. Statistics

Statistical analyses were performed in SigmaPlot v.14 (Systat Software GmbH). Significant differences between variable groups were evaluated by Student's and Welch's t-tests, Mann-Whitney rank sum test, and one-way analysis of variance (ANOVA) with subsequent post-hoc tests for multiple comparisons (Holm-Sidak's method). Normality of data and homogeneity of variances were analyzed using the Shapiro-Wilk and Brown-Forsythe test, respectively. For non-normally distributed data, we used Kruskal-Wallis one-way ANOVA on ranks with subsequent Tukey post-hoc tests for multiple comparisons. Differences of means/medians were considered significant at $p < 0.05$. Correlations were evaluated based on Pearson's product moment coefficient (r_p) or Spearman's rank correlation coefficient (r_s) if data were not normally distributed. Depending on methodology, statistical tests involved a variable number of observations (N).

3. Results

3.1. Solution trends

Changes in E_h and pH values during redox oscillations are illustrated in Fig. 2. Redox potentials declined after submergence and leveled off between approximately zero and -250 mV after 7 days. Median E_h values of all reduction cycles in the 14-day cycle experiment differed only significantly between the low- and high-OC treatments (control = -127 mV, low-OC = -157 mV, high-OC = -103 mV; N = 48), which was also the case for the 28-day cycle experiment (control = -98 mV, low-OC = -114 mV, high-OC = -71 mV; N = 40). During anoxia,

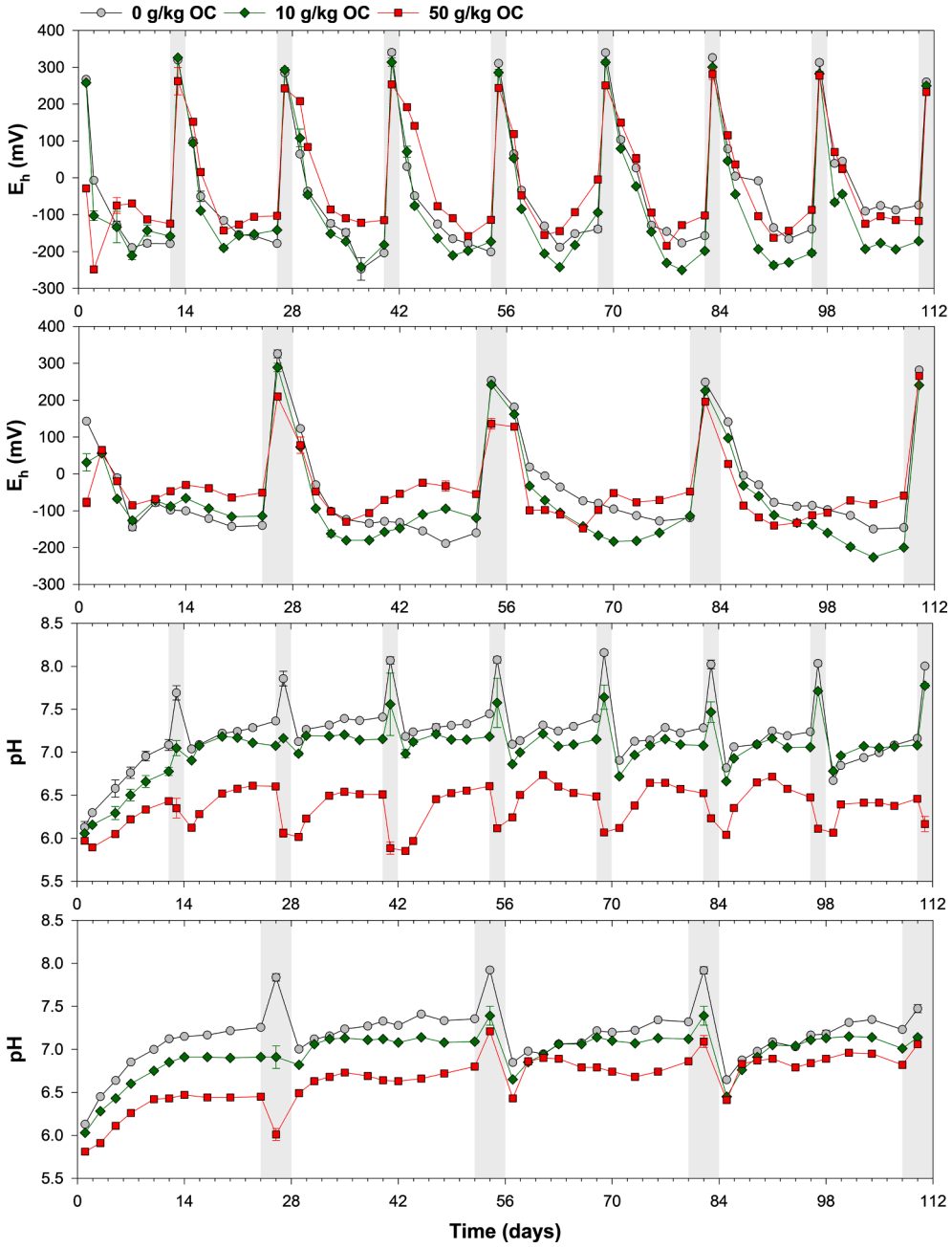

Fig. 2. Evolution of E_h and pH in the 14- and 28-day cycle experiments with soil amended with 0, 10, and 50 g/kg straw-OC. For each dependent parameter, the upper panel refers to the 14-day cycle experiment. The legend is valid for all panels. Oxidation periods are shown in gray. Data of oxidation periods originate from anoxic soil solutions, which were obtained by centrifugation and oxidized in ambient air for 48 h. Data points are connected for clarity. Error bars denote standard deviation of triplicate experiments. Note that reacted solutions were removed from soils at the end of each reduction period and preplaced by fresh artificial river water.

pH values continuously increased by up to 1.1 pH unit. These increases were less pronounced with increasing straw additions (Fig. 2). Generally, median pH values of all reduction periods differed significantly between all treatments of the 14-day cycle (control = 7.2, low-OC = 7.1, high-OC = 6.5) and 28-day cycle experiment (control = 7.2, low-OC = 7.1, high-OC = 6.7).

Fig. 3 shows the evolution of DOC and Fe_{aq} concentrations as well as the Fe(II) fraction of Fe_{aq}. Reducing conditions increased DOC concentrations, and the amount of DOC released upon soil reduction increased with increasing straw additions. Median DOC concentrations of all reduction periods differed significantly between all treatments in both redox experiments (f_{redox} = 14 days/cycle: control = 7.2 mM, low-OC = 14.5 mM, high-OC = 48.1 mM and f_{redox} = 28 days/cycle: control = 12.1 mM, low-OC = 20.4 mM, high-OC = 52.1 mM). Concentrations of DOC declined during consecutive reduction periods, and showed pronounced maxima during each reduction step in the 28-day cycle experiment (Fig. 3).

Dissolved Fe concentrations increased approximately linearly during reduction periods, with the exception of the high-OC treatment in the 28-day cycle experiment, where they plateaued at earlier and earlier times during each successive reduction period (Fig. 3). The amount of Fe_{aq} released during reduction periods also increased with increasing straw additions. Median Fe_{aq} concentrations of all reduction periods differed significantly between all treatments in both redox experiments (f_{redox} = 14 days/cycle: control = 0.18 mM, low-OC = 0.58 mM, high-OC = 1.73 mM and f_{redox} = 28 days/cycle: control = 0.24 mM, low-OC = 0.89 mM, high-OC = 1.84 mM). Similar to DOC concentrations, Fe_{aq} concentrations also decreased during consecutive reduction

periods; these decreases were also more pronounced in the 28-day cycle experiment (Fig. 3). Fig. 3 also shows that the majority of Fe_{aq} was present as Fe(II). However, particularly at the onset of reduction periods, substantial amounts of Fe(III) were released into solution, most likely as organic Fe(III) complexes or inorganic Fe(III) colloids < 200 nm.

We calculated average DOC and Fe_{aq} release rates for each reduction period from initial concentration ranges using linear regressions (Fig. 4). These data show that DOC release rates dropped significantly during soil redox cycling at both redox frequencies in the straw treatments, but remained constant within error for the control treatments. For the straw treatments, the decline in DOC release rate per redox cycle was more pronounced in the 28-day cycle experiment (Fig. 4). Likewise, Fe_{aq} release rates only decreased in straw treatments at $p \leq 0.1$, which was also slightly more evident in the 28-day cycle experiment (Fig. 4). Because DOC and Fe_{aq} release rates followed similar trends, both rates were highly correlated (Fig. 5).

Cumulative DOC and Fe_{aq} losses from soil, calculated from aqueous concentrations and average gravimetric water contents before soil oxidation, are displayed for both redox experiments in Fig. 6. In each treatment, cumulative DOC and Fe_{aq} losses were highly correlated ($r_p = 0.99$, $p < 0.01$). Losses of DOC were up to 6-fold and of Fe_{aq} up to 10-fold higher in straw-amended soils relative to the controls after the last reduction cycle. Fig. 6 additionally shows that redox frequency had a marked influence on reduction-induced DOC and Fe_{aq} losses after the final reduction period: For the low-OC treatments, up to 28 % more DOC and 24 % more Fe_{aq} were lost from the system in the 14-day cycle than in the 28-day cycle experiment, whereas for the high-OC treatments, DOC

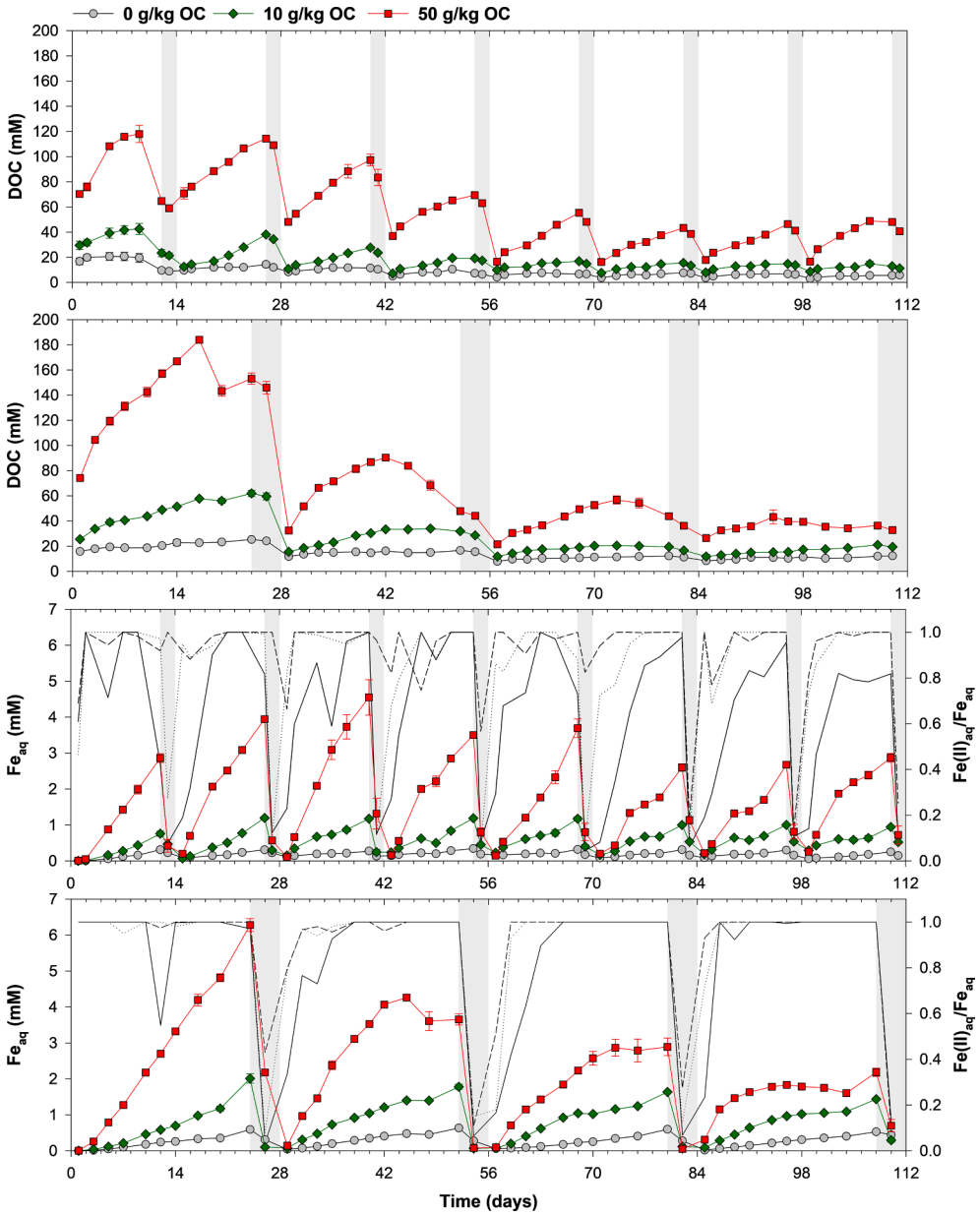

Fig. 3. Evolution of DOC, dissolved Fe, and the Fe(II) fraction of dissolved Fe in in the 14- and 28-day cycle experiments with soil amended with 0, 10, and 50 g/kg straw-OC. For each dependent parameter, the upper panel refers to the 14-day cycle experiment. The legend is valid for all panels. Oxidation periods are shown in gray. Black lines refer to $Fe(II)_{aq}/Fe_{aq}$ ratio (solid: 0 g/kg OC, dotted: 10 g/kg OC, dashed: 50 g/kg OC). Data of oxidation periods originate from anoxic soil solutions, which were obtained by centrifugation and oxidized in ambient air for 48 h. Data points are connected for clarity. Error bars denote standard deviation of triplicate experiments. Note that reacted solutions were removed from soils at the end of each reduction period and preplaced by fresh artificial river water. Concentration trends of dissolved Si can be found in Figure S15.

and Fe_{aq} losses were nearly twice as high in the 14-day cycle than in the 28-day cycle experiments. Absolute Fe losses from soils amounted to ≤ 1.6 % of Fe_{tot} in the control and low-OC treatments and ≤ 4.4 % of Fe_{tot} in the high-OC treatments.

3.2. Iron speciation changes in bulk soil

3.2.1. Selective extractions

Selective extractions were used to investigate the effect of straw OC level as well as redox frequency and time on the composition of soil Fe pools. Because straw additions reduced the Fe_{tot} content per unit soil mass by 2.8 and 12.5 % in the low- and high-OC treatments, respectively, only changes in absolute extractable Fe parameters beyond these values will be detailed. First, we evaluated the effect of straw OC for both redox experiments (f_{redox} = 14 and 28 days/cycle) by comparing time series means of specific extraction parameters of re-oxidized soil samples for each of the two redox experiments with straw-OC as categorical predictor variable using one-way ANOVA. For the 14-day cycle experiment, we found significantly lower values of Fe_o, Fe_o–Fe_p, Fe_o/Fe_{tot}, (Fe_o–Fe_p)/Fe_{tot}, and Fe_o/Fe_d as well as significantly higher ratios of Fe_d/Fe_{tot} and Fe_p/Fe_{tot} in straw-amended soil (Table S1). Post-hoc tests revealed that these effects were mainly caused by differences between the high-OC treatment and the low-OC treatments (Table S1). This is exemplified by Fig. 7 illustrating trends in Fe_o/Fe_d ratio—an indicator of Fe-oxide crystallinity—in both redox experiments. In the 14-day cycle experiment, only the Fe_o/Fe_d ratio in the control and low-OC treatments increased beyond that of the original soil, whereas in the 28-day cycle experiment, the Fe_o/Fe_d ratio of all treatments remained unchanged. In the 28-day cycle experiment, we generally found similar effects of straw OC on extractable Fe parameters, except that there was no effect of OC level on Fe_d/Fe_{tot} and Fe_p/Fe_{tot} ratios (Table S1). Here, even the low-OC treatment significantly decreased the Fe_o/Fe_{tot} ratio, and there was no difference in Fe_o/Fe_{tot} ratio between the low- and high-OC treatments (Table S1).

Considering Fe budgets in both redox experiments, we noticed that, accounting for soil dilution by straw, the highest OC additions led to a mean loss of only up to 445 mg/kg Fe_o, but up to 1120 mg/kg Fe_o–Fe_p after 112 days when compared to the redox-cycled controls (4 and 19 % difference, respectively). The higher losses of Fe_o–Fe_p compared to Fe_o suggest that SRO Fe oxides dissolved disproportionally compared to organic Fe(III) complexes during 112 days. During this time, the mean Fe_o/Fe_d ratio of straw treatments decreased by up to 10 % relative to the controls (Table S1). This effect originated from significantly higher Fe_o/Fe_d ratios in the controls compared to the high-straw treatments (Fig. 7, Table S1), showing that high straw additions impaired the accumulation of SRO Fe oxides during soil redox cycling.

Next, we tested for the effects of redox frequency on extractable Fe parameters and compared mean values of extractable Fe parameters determined in both redox experiments after 28, 56, 84, and 112 days for each OC treatment. These results showed that in the control treatment of the 28-day cycle experiment, the values of Fe_d and Fe_d/Fe_{tot} were 7 and 5 % higher, respectively, and the Fe_o/Fe_d ratio was 8 % lower than in the 14-day cycle experiment (Table S2). Similar trends were observed for the low-OC treatments, but unlike the controls, the mean Fe_o/Fe_{tot} ratio

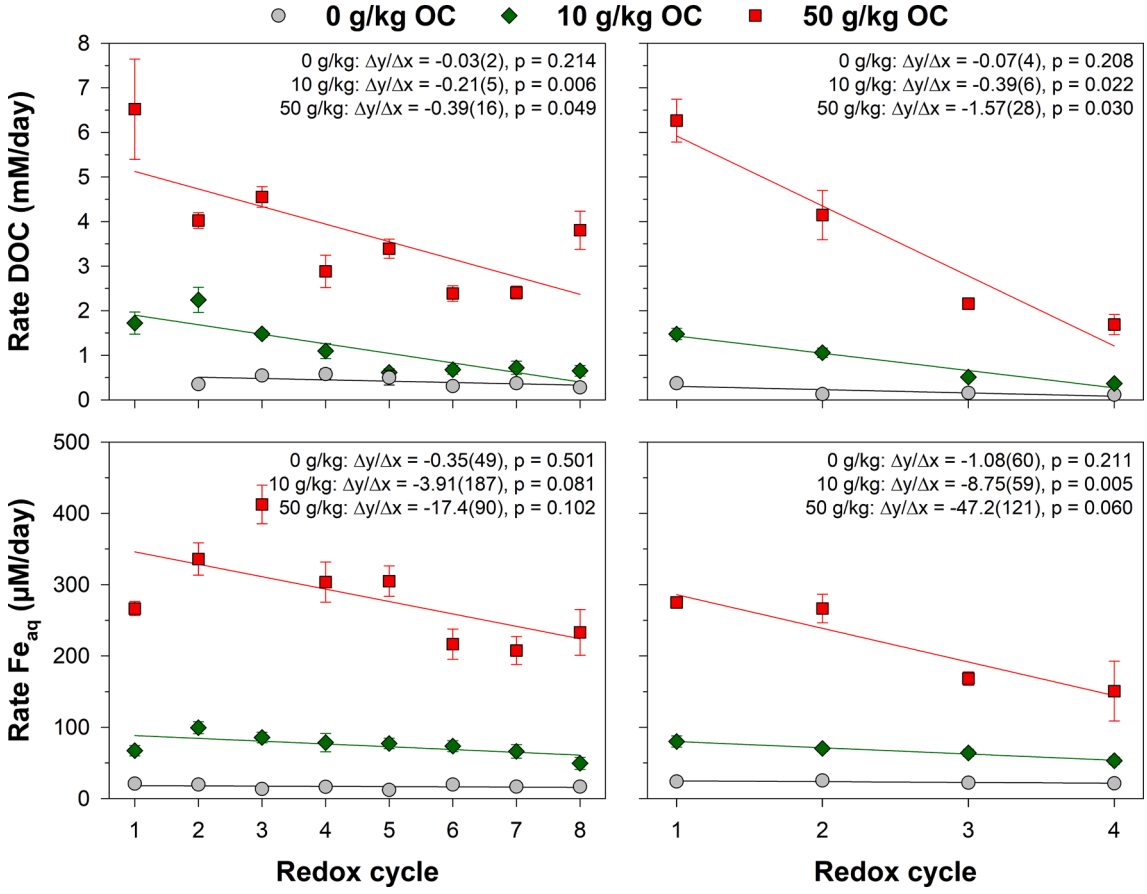

Fig. 4. Changes in DOC and Fe_{aq} release rates during reduction periods in the 14-day cycle (left) and 28-day cycle experiments (right) with soil amended with 0, 10, and 50 g/kg straw-OC. Each redox cycle of the 14-day cycle (28-day cycle) experiment included a reduction and oxidation period of 12 and 2 days (24 and 4 days), respectively. Error bars denote standard errors. Lines are linear regressions whose slope parameters are reported in each panel. Numbers in parentheses give the standard error for the last digit.

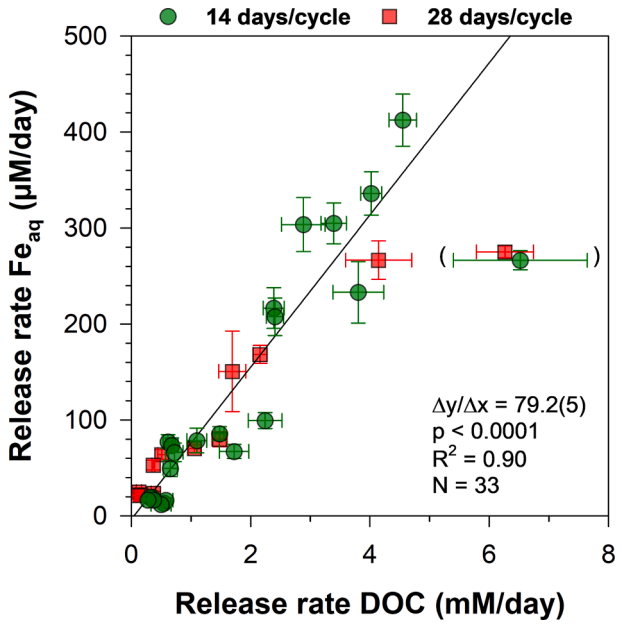

Fig. 5. Regression of Fe_{aq} against DOC release rates during soil reduction periods in the 14-and 28-day cycle experiments with soil amended with 0, 10, and 50 g/kg straw-OC. Each redox cycle of the 14-day cycle (28-day cycle) experiment included a reduction and oxidation period of 12 and 2 days (24 and 4 days), respectively. Error bars denote standard errors. The two data points on the far right were excluded from regression, as they were influenced by high DOC flushes in the 50 g/kg OC treatments during the first reduction period. The standard error of the regression slope applies to the last digit.

was also 4 % lower in the 28-day cycle experiment. At the highest OC level, redox frequency had no significant effect on any of the extractable Fe parameters (Table S2).

To investigate the effect of experimental duration on extractable Fe parameters for the 14-day cycle experiment, each time series was divided into two time intervals (0–56 and 56–112 days) and the interval means compared for each OC treatment. In this way, we compared mean values of samples exposed to redox cycles for 56 days with those exposed for twice as long. Significant effects of time were only observed for the control and high-OC treatments. In the control, we found a decrease in Fe_o–Fe_p (by 12 %) and (Fe_o–Fe_p)/Fe_{tot} (by 11 %) values with longer redox cycling, implying progressive dissolution of SRO Fe oxides. In the high-OC treatment, Fe_d, Fe_o, Fe_d/Fe_{tot}, and Fe_o/Fe_{tot} values decreased by ~ 5 % between the first and second time interval (Table S3).

3.2.2. X-ray absorption spectroscopy

XANES spectra of the original soil and all re-oxidized soil samples of the 14-day cycle experiment were analyzed for the oxidation state of Fe using goethite, ferrihydrite, and Fe(II)-oxalate dihydrate as fit references. The fit of the original soil is shown in Figure S1 as an example, and Table S4 summarizes all fit results. Accordingly, the original soil contained 17 % Fe(II), suggesting that a significant portion of Fe was present in Fe(II)-bearing silicates. During soil redox cycling for 112 days, Fe(II) contents in re-oxidized soil samples never exceeded 20 % ($\bar{x}$ = 18 %) and there were also no significant differences in time series means of Fe(II) content between all OC treatments (ANOVA, p = 0.394).

To identify suitable reference spectra for EXAFS LCF, soil spectra were analyzed by principal component analysis and target-transformation testing in Athena (Mikutta and Rothwell, 2016; Scheinost et al., 2002). These analyses were inconclusive because only one component explaining 99 % of spectral variance could be identified. Therefore, reference selection was based on a priori knowledge. Selective extractions implied the presence of organically bound Fe as well as SRO and well crystallized Fe oxides. Soil EXAFS spectra showed features of hematite (α-Fe_2O_3) and the presence of Fe(II) in the original soil suggested a considerable portion of Fe bound in Fe(II)-bearing silicates. In contrast to ferrihydrite, lepidocrocite (γ-FeOOH), and hematite, goethite always contributed insignificantly (< 5 %) to the fits. Eventually, all soil spectra could be well fit with a combination of Fe(III)-citrate—representative of Fe(III) complexed by COOH/OH groups of organic ligands—ferrihydrite, lepidocrocite, hematite, biotite, and muscovite.

Selected Fe K-edge EXAFS spectra and their LCFs of re-oxidized soil samples of the 14-day cycle experiment are shown in Fig. 8 along with reference spectra used for LCF. Fig. 8 documents subtle changes in the local Fe coordination of bulk soil samples as a function of the number of redox cycles and OC level. EXAFS spectra of soil samples subject to redox fluctuations became progressively dissimilar to that of the original soil with increasing number of redox cycles, with the least changes observed in the high-OC treatment (Fig. 8). According to the LCF results (Table 2), the original soil contained approximately 21 % organically complexed Fe(III), 53 % Fe oxides (34 % ferrihydrite, 11 % hematite, and 7 % lepidocrocite), and 26 % Fe bound in silicate structures (18 % biotite and 8 % muscovite). The high fraction of biotite agrees well with 17 % Fe(II) estimated from XANES LCF. In all samples analyzed, its fraction showed a positive correlation with Fe(II) content (r_p = 0.61, p = 0.001, N = 25), while there was no correlation with muscovite (p = 0.141). This result suggests that Fe(II) in the original soil and re-oxidized soil samples was primarily associated with biotite or Fe(II)-rich clay minerals.

Redox-cycled soil samples (N = 24) exhibited considerable variation in major Fe species, which may be caused by the intrinsic soil heterogeneity (Table 2). The fraction of organically complexed Fe(III) varied from 14 to 24 % ($\bar{x}$ = 20 %) and that of ferrihydrite from 30 to 38 % ($\bar{x}$ = 34 %). The fraction of Fe oxides (ferrihydrite, hematite, and lepidocrocite) accounted for 45–53 % of Fe_{tot} ($\bar{x}$ = 49 %). Biotite and muscovite fractions contributed 14–20 % ($\bar{x}$ = 17 %) and 9–18 % ($\bar{x}$ = 14 %) to Fe_{tot}, respectively. Their fractions summed up to 28–34 % ($\bar{x}$ = 31 %) (Table 2). Most noticeably, redox-cycled soils had almost twice as much muscovite-Fe as the original soil, implying a relative enrichment of Fe-poor phyllosilicates in redox-cycled soils.

Based on LCF results, a one-way ANOVA was performed to compare the effect of OC level on the mean values of individual solid-phase Fe species within the 14-day cycle experiment. This analysis revealed a significant difference in the fraction of organically complexed Fe(III) (Table S5). Post-hoc tests showed that the mean fraction of organically complexed Fe(III) was higher in the low- and high-OC treatments compared to the control (by 13 and 28 %, respectively) and was also higher in the high-OC compared to low-OC treatment (by 13 %) (Table S5). Additionally, we found a significant difference in the mean ferrihydrite fraction. Post-hoc tests revealed a lower mean ferrihydrite fraction in the high-OC treatment compared to the control (by 7 %), while there was no difference between the low-OC treatment and the control and high-OC treatments (Table S5). For the total Fe-oxide fraction, we also detected a significant effect of OC level. This fraction decreased in both straw treatments compared to the control (by ~ 7 %), while differences between the straw treatments were insignificant (Table S5). Phyllosilicate fractions were not significantly affected by OC level during redox oscillations.

Analogous to our selective extraction results, we explored the effect of time on Fe species quantified by EXAFS LCF for each OC level in the 14-day cycle experiment. For the control treatment, we found no effect of time on time-interval means (0–56 vs. 56–112 days) of any Fe species. For the low- and high-OC treatments, we only detected a significant decline in mean Fe-oxide fractions between both time intervals (by ~ 5 %) (Table S6).

3.2.3. Mössbauer spectroscopy

Mössbauer spectra were collected at 295, 77, and 5 K for the original soil and re-oxidized soil samples of all OC treatments cycled for 56 and 112 days at f_{redox} = 14 and 28 days/cycle (N = 13). Fig. 9 illustrates MB spectra of the original soil collected at all three temperatures. Spectral

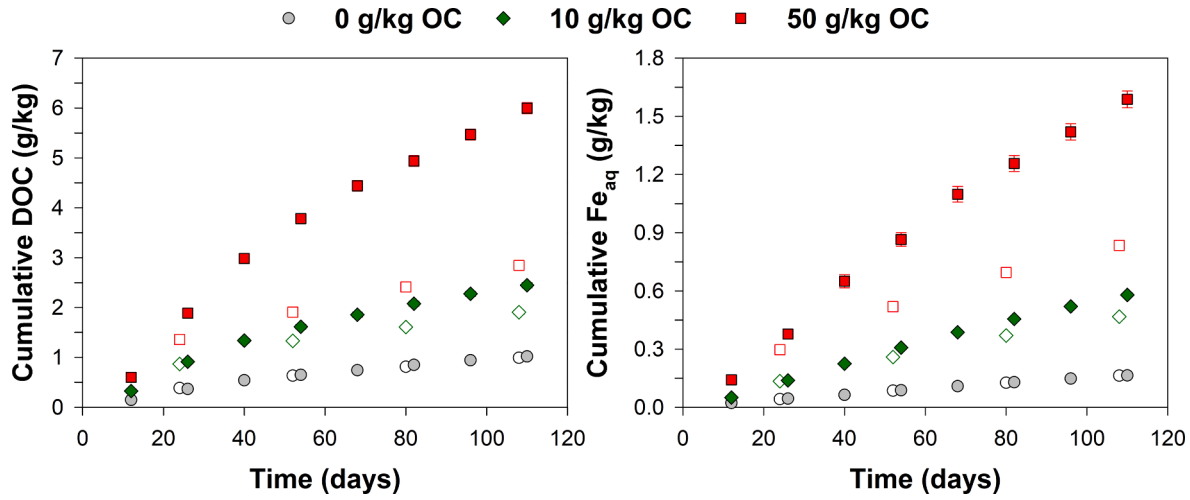

Fig. 6. Cumulative DOC and Fe losses per kilogram straw-free soil (dry-weight basis) during soil reduction periods in the 14-day cycle (filled symbols) and 28-day cycle experiments (open symbols) with soil amended with 0, 10, and 50 g/kg straw-OC. Each redox cycle of the 14-day cycle (28-day cycle) experiment included a reduction and oxidation period of 12 and 2 days (24 and 4 days), respectively. Error bars denoting propagated standard deviations are mostly smaller than the symbol size.

components resolved in MB spectra collected at all temperatures included: (1) an Fe(III) quadrupole doublet (Q-Fe(III)), which corresponds to Fe(III) in surface complexes, silicates, and Fe oxides superparamagnetic at the temperature of collection, (2) an Fe(II) quadrupole doublet (Q-Fe(II)) representing Fe(II) in silicate minerals (with partial magnetic ordering at 5 K, then designated H-(b)Fe(II)), (3) a broadened Fe(III) sextet (H-OxHy) corresponding to magnetically ordered ferrihydrite and lepidocrocite, (4) a partially collapsed Fe(III) sextet (H-(b)OxHy) representing Fe(III) species with blocking temperatures near the temperature of collection, and (5) a broad Fe(III) sextet (H-Ox) assigned to hematite.

In the following, we mainly address Fe speciation based on the 5-K spectra, the results of which are summarized in Table 3. Corresponding data of the 295- and 77-K spectra as well as MB parameters of all spectra can be found in the Supplementary material. For the original soil, Q-Fe(III) accounted for 15 %, the sum of Q-Fe(II) and H-(b)Fe(II) for 13 %, H-OxHy for 37 %, H-(b)OxHy for 24 %, and H-Ox for 11 % of spectral area at 5 K (Table 3). Assuming that at 5 K all Fe oxides are magnetically ordered, Q-Fe(III) at 5 K would nominally correspond to mononuclear organic Fe(III) complexes and Fe(III) in Fe-poor silicates. However, the Q-Fe(III) component represented only 15 % of spectral area, which was lower than the 21 % of organically complexed Fe(III) determined by XAS. Assigning the 8 % muscovite-Fe (XAS) to the Q-Fe(III) pool implies that only one third of organically complexed Fe (III) determined by XAS was mononuclear Fe(III) and the rest present as polynuclear Fe(III) complexes (Hoffmann et al., 2013; Mikutta and Kretzschmar, 2011). This accords with Fe EXAFS shell-fit and wavelet-transform results obtained for our Fe(III)-citrate reference indicating second-shell Fe at 3.34(3) Å (Fig. S2). The Fe(II) content of 15 %, taken from the spectral area of the Q-Fe(II) component at 295 K (Table S8), agreed well with the 17 % of Fe(II) and the 18 % biotite quantified by XAS. Likewise, the 11 % area of the Ox sextet representing hematite was consistent with the 11 % hematite determined by XAS (Tables 2 and 3). The sum area of Fe(III) sextets OxHy and Ox (48 %) originating from distinct Fe oxides matched well with the sum of ferrihydrite, hematite, and lepidocrocite determined by EXAFS spectroscopy (53 %). Consequently, the partially collapsed sextets at 5 K (H-(b)OxHy) likely does not *sensu stricto* represent the 'most disordered Fe oxides' (Chen et al., 2019; Giannetta et al., 2022). This is because (1) even the least ordered ferrihydrites possess a local (< 5 Å) ferrihydrite structure (Mikutta,

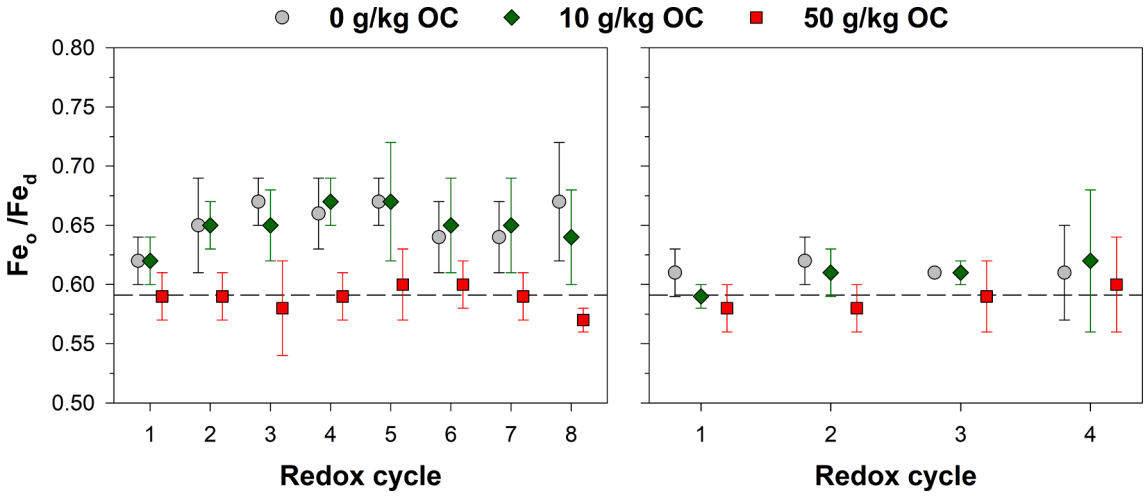

Fig. 7. Changes in Fe_o/Fe_d ratio as a measure of crystallinity of pedogenic Fe oxides in the 14- and 28-day cycle experiments with soil amended with 0, 10, and 50 g/kg straw-OC. Each redox cycle of the 14-day cycle (28-day cycle) experiment included a reduction and oxidation period of 12 and 2 days (24 and 4 days), respectively. Error bars denote standard deviations calculated from those of triplicate Fe_o and Fe_d measurements. The dashed lines mark the Fe_o/Fe_d ratio of the original soil (0.59(4)). Data were offset for clarity.

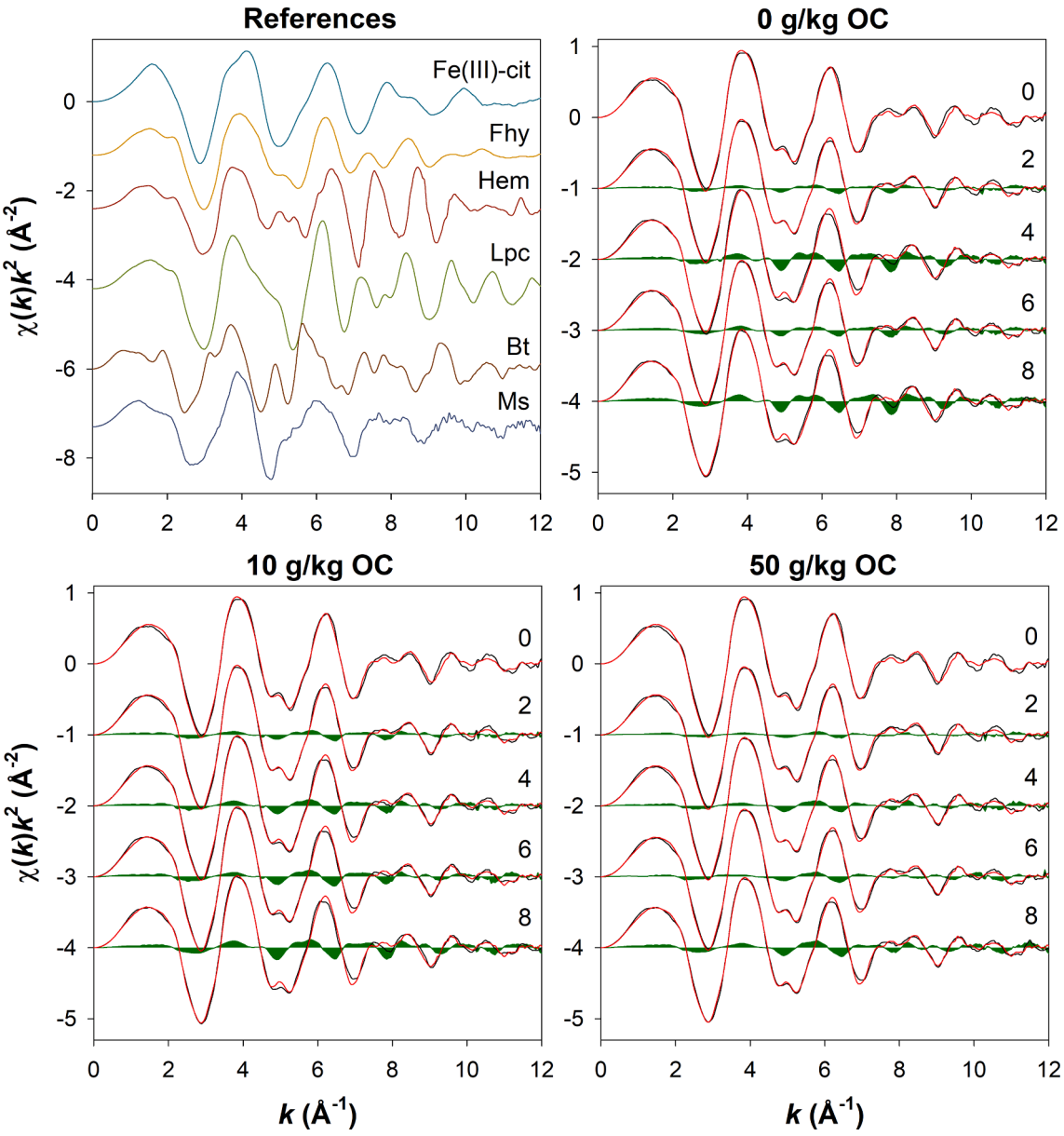

Fig. 8. Iron K-edge EXAFS spectra ($E_0 = 7130$ eV) of reference compounds and re-oxidized soil samples (black lines) amended with 0, 10, and 50 g/kg straw-OC and subjected to 0, 2, 4, 6, and 8 redox cycles at $f_{redox} = 14$ days/cycle. Each redox cycle included a reduction and oxidation period of 12 and 2 days, respectively. Linear combination fits are shown as red lines. The spectra for cycle 0 refer to the original soil. Green shaded areas depict spectral differences calculated by subtracting the original soil spectrum from each other spectrum. References: Fe(III)-cit = Fe(III)-citrate, Fhy = ferrihydrite, Hem = hematite, Lpc = lepidocrocite, Bt = biotite, Ms = muscovite. Fit results are presented in Table 2.

2011), rendering them well quantifiable by XAS, and (2) disordered ferrihydrites formed via coprecipitation with DOC (molar $C/Fe_{solid} \leq 0.54$) are fully magnetically ordered at 5 K (Eusterhues et al., 2011). Therefore, we interpret the H-(b)OxHy MB component here as Fe(III) domains with dimensions of only a few Ångstrom, such as those present in polynuclear organic Fe(III) complexes (Hoffmann et al., 2013; Mikutta and Kretzschmar, 2011). Our reasoning is supported by a relatively close correspondence between the H-(b)OxHy component (24 %) and the sum of XAS-derived organic Fe(III) complexes not explained by MBS (Δ14%) and distinct Fe oxides identified by XAS but not explained by MBS (sum of H-OxHy and H-Ox, Δ5%) (Tables 2 and 3). Given that XAS likely underestimated the fraction of mononuclear organic Fe(III) complexes due to the low scattering amplitude of carbon atoms, the H-(b)OxHy MB component could be entirely ascribed to Fe(III) in polynuclear organic complexes in our samples. A positive correlation of the proportion of H-(b)OxHy with the Fe_p/Fe_{tot} ratio (fraction of organically complexed Fe; $r_p = 0.58$, $p = 0.037$, $N = 13$) and a negative correlation with the $(Fe_o–Fe_p)/Fe_{tot}$ ratio (fraction of ferrihydrite; $r_p = -0.62$, $p = 0.025$, $N = 13$) further supports the notion that the H-(b)OxHy MB component better reflects polynuclear organic Fe(III) complexes than SRO Fe oxides in our samples. According to XAS and MB reconciliation, the H-(b)OxHy MB component consisted of at least 70 % polymerized Fe(III) in organic complexes and at most 30 % Fe(III) of nanoscale Fe oxides, perhaps Fe (III) of distorted surface shells of extremely small ferrihydrite particles (Hiemstra, 2013). For simplicity, we collectively refer to the H-(b)OxHy MB component as 'very short-range ordered' (vSRO) Fe(III) solids in order to distinguish it from ferrihydrite, which at 5 K mainly contributes to the H-OxHy MB fraction. Regardless of the exact nature of the H-(b)OxHy MB component, the crystallinity index of distinct Fe oxides (ferrihydrite, lepidocrocite, and hematite) calculated as sum area ratio of OxHy and Ox sextets at 77 and 5 K, was 0.65 (Table 3), which implies

Table 2
Fit fractions (%) of Fe reference compounds used for EXAFS-LCF analysis of the original soil and re-oxidized soil samples of the 14-day cycle experiment.[a]

Cycle	Fe(III)-cit	Fhy	Hem	Lpc	Ms	Bt	Fit sum	*R*-factor ($\times 10^3$)[b]	red. χ^2 ($\times 10^3$)[c]
					Original soil				
0	21	34	11	7	8	18	1.01	8.3	1.6
					0 g/kg OC				
1	16	38	9	6	16	15	1.04	7.0	1.4
2	19	35	10	7	11	18	1.03	4.4	0.9
3	19	34	8	7	14	17	1.02	4.8	1.0
4	18	33	8	9	18	14	1.00	9.3	1.9
5	19	36	9	5	11	20	1.02	4.0	0.8
6	18	36	10	7	13	17	1.03	3.3	0.7
7	14	38	8	6	17	16	1.04	8.6	1.8
8	14	37	8	7	18	15	1.04	8.5	1.8
					10 g/kg OC				
1	17	36	8	6	17	16	1.02	6.7	1.3
2	19	35	9	6	12	19	1.03	3.9	0.8
3	19	36	7	6	16	17	1.03	9.1	1.9
4	20	34	8	6	13	18	1.04	4.9	1.0
5	24	30	10	7	10	20	1.01	6.1	1.2
6	20	34	8	6	14	18	1.03	5.0	1.0
7	20	35	6	6	16	17	1.03	9.6	2.0
8	18	34	8	6	17	17	1.05	8.7	1.8
					50 g/kg OC				
1	18	38	9	5	12	18	1.02	4.1	0.8
2	24	33	10	6	9	19	1.02	6.3	1.3
3	21	35	7	6	15	16	1.04	7.1	1.5
4	24	32	8	6	11	18	1.02	4.5	0.9
5	23	33	8	6	13	18	1.03	4.3	0.9
6	24	32	9	5	11	19	1.01	3.8	0.7
7	22	32	7	6	17	16	1.02	9.2	1.9
8	22	32	8	6	14	18	1.03	4.2	0.9

[a] Fit fractions were recalculated to 100 %. Relative uncertainties of fit fractions are 10 % at best. Reference compounds: Fe(III)-cit = Fe(III)-citrate, Fhy = ferrihydrite, Hem = hematite, Lpc = lepidocrocite, Ms = muscovite, Bt = biotite.

[b] $R\text{-factor} = \Sigma_i(\text{data}_i - \text{fit}_i)^2 \,/\, \Sigma_i \text{data}_i$.

[c] Reduced $\chi^2 = (N_{idp}/N_{pts})\Sigma_i((\text{data}_i - \text{fit}_i)/\varepsilon_i)^2(N_{idp} - N_{var})^{-1}$, where N_{idp} is the number of independent points in the model fit, N_{pts} the total number of data points, N_{var} the number of fit variables in the final fit, and ε_i the uncertainty of the i^{th} data point.

a moderate crystallinity of Fe oxides.

Fig. 10 illustrates 5-K MB spectra of re-oxidized soil samples amended with 0, 10, and 50 g/kg straw-OC after 112 days of redox cycling at $f_{redox} = 14$ days/cycle. The figure demonstrates marked changes in spectral composition as a function of OC content, especially a decrease in spectral area of the OxHy sextet with increasing OC level. Spectral analyses showed that, compared to the original soil, the fraction of mononuclear organic Fe(III) complexes and Fe(III) in low-Fe silicates (Q-Fe(III)) increased in all redox-cycled soils by as much as 7 % in the high-OC treatments (41 % relative change). Simultaneously, the fraction of distinct Fe oxides (H-OxHy + H-Ox) declined from 48 % in the original soil to 35 % in the redox-cycled soils (-28 % relative change). This decrease was more pronounced with increasing OC addition (Table 3). For the H-(b)OxHy component, we noted no changes in the control treatments relative to the original soil, and absolute increases of up to 7 % in the straw treatments relative to the controls after 112 days (29 % relative change; Table 3). Additionally, we found no marked changes in Fe(II) (Q-Fe(II) and H-(b)Fe(II)) and hematite (H-Ox) contents in re-oxidized soil samples, consistent with XAS (Tables 2, 3, and S4). In summary, 5-K MB data for all soil samples redox-cycled for 112 days showed that the proportion of organic Fe(III) complexes increased and the proportion of distinct Fe oxides decreased, with stronger changes occurring in straw-amended soils. The decreased proportion of distinct Fe oxides was accompanied by marked increases in their crystallinity, as evidenced by the increase in crystallinity indices from 0.65 (original soil) up to 0.80 (controls), 0.87 (low-OC treatments), and 0.96 (high-OC treatments) after 112 days (Table 3).

Redox frequency ($f_{redox} = 14$ vs. 28 days/cycle) had a marginal impact (<5%) on MB-derived Fe speciation. The lower redox frequency increased the crystallinity index of distinct Fe oxides in the control treatments (0.73 to 0.80), whereas redox frequency had no impact on their crystallinity in straw-amended soils after 112 days (Table 3). Similarly, the effect of redox fluctuation time (56 vs. 112 days) on MB-Fe speciation was small. The crystallinity index of distinct Fe oxides increased with time at both redox frequencies, and these increases were greater at lower redox frequency and most pronounced in the high-OC treatments (0.85 to 0.95) (Table 3).

3.3. Relation between solution parameters and solid-phase Fe speciation

We tested for all significant correlations between solid-phase Fe speciation present at the onset of reduction periods and DOC and Fe_{aq} releases as well as maximal changes of solution pH (ΔpH) during all reduction phases. The increase of soil pH was positively correlated with the 5-K H-OxHy MB component (ferrihydrite and lepidocrocite) ($r_s = 0.82$, $p < 0.0001$, $N = 12$) and negatively with the 5-K Q-Fe(III) MB component (Fe(III) in organic complexes and low-Fe silicates) ($r_s = -0.80$, $p < 0.001$, $N = 12$). This suggests that higher initial Fe-oxide contents resulted in a higher proton consumption due to microbial Fe reduction and that OM either buffered pH and/or limited Fe reduction. Release rates of DOC were positively related to the Fe(III)-citrate fraction determined by XAS ($r_s = 0.73$, $p < 0.0001$, $N = 23$) and negatively to Fe_o ($r_s = -0.72$, $p < 0.0001$, $N = 35$) and the XAS-derived ferrihydrite content ($r_s = -0.54$, $p < 0.01$, $N = 23$). Maximum DOC concentrations during reduction periods and DOC concentrations at the end of reduction periods were also positively correlated with the XAS-derived Fe(III)-citrate fraction ($r_s = 0.74$ and 0.70, respectively, $p \leq 0.0001$, $N = 24$), whereas they were negatively related to Fe_o and Fe_o/Fe_d ratio ($r_s = -0.70$ to -0.82, $p < 0.0001$, $N = 36$). Similarly, Fe release rates were positively correlated with Fe(III)-citrate fractions determined by XAS ($r_s = 0.70$, $p = 0.0001$, $N = 24$) and negatively with Fe_o ($r_s = -0.78$, $p < 0.0001$, $N = 36$). Combined, these results may suggest SRO Fe oxides stabilized OC against reductive release, that Fe release under reducing conditions was enhanced by organic Fe(III) complexes, and that reduction of Fe(III) in these complexes contributed to DOC production.

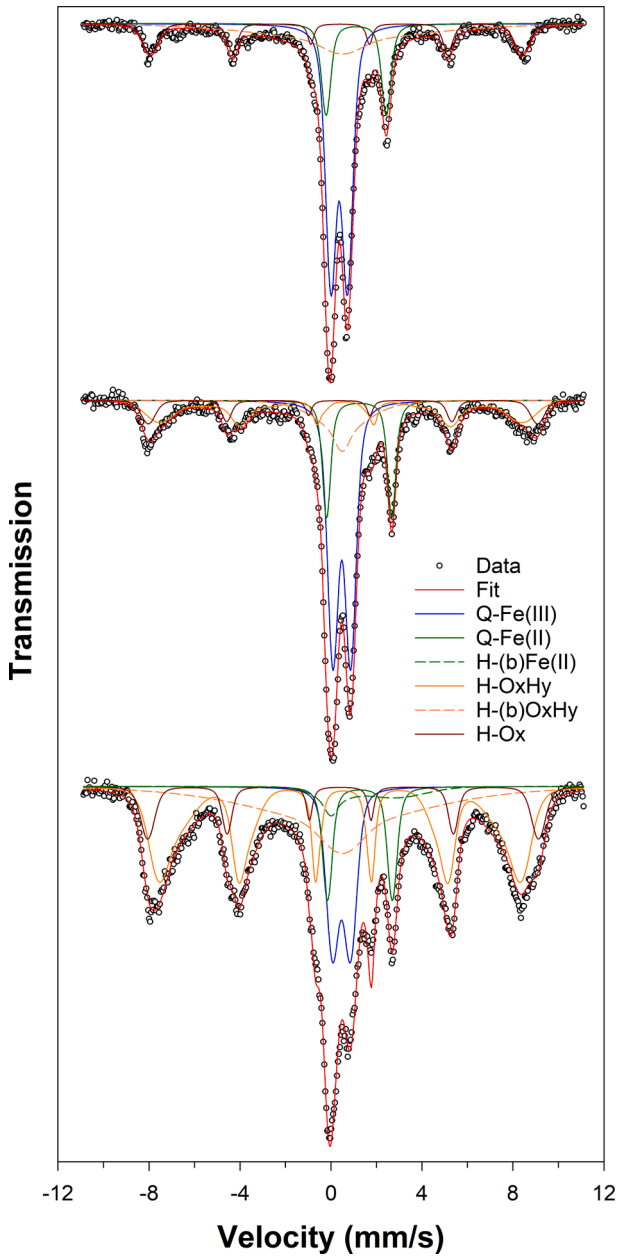

Fig. 9. ^{57}Iron Mössbauer spectra collected at 295, 77, and 5 K (top-down) of the original soil. Component interpretation: Q-Fe(III) = mononuclear organic Fe(III) complexes and Fe(III) in low-Fe silicates, Q-Fe(II) and H-(b)Fe(II) = silicate-bound Fe(II), H-OxHy = Fe(III) oxyhydroxides and ferrihydrite, H-(b)OxHy = Fe(III) species with very short-range order ('vSRO Fe(III) solids'), H-Ox = hematite. Fit results are presented in Tables 3, S7, and S8. Additional spectra are shown in Figures S3-14.

4. Discussion

4.1. Solution trends

Soil reduction typically increases DOC concentrations as a result of increased biological activity, reductive OC release from Fe and Mn oxides, and pH-driven OC desorption from mineral host phases (Grybos et al., 2009) or dispersion of small OC-bearing colloids (Buettner et al., 2014). High correlations between DOC and Fe release rates, cumulative DOC and Fe_{aq} releases (Figs. 5 and 6), and a negative correlation between pH and DOC concentration (r_p = -0.57, $p < 0.0001$, N = 264) imply that straw additives were the major source of DOC, which stimulated the activity of Fe(III) reducers and thus promoted the bioreduction of Fe(III) solids. Simultaneously, straw amendments released substantial amounts of Si into solution (Fig. S15), resulting in a high positive correlation between DOC and dissolved Si ($r_p = 0.74$, $p < 0.0001$, N = 264). Declining rates of DOC production with advancing redox cycling in straw-amended soils (Figs. 3 and 4) imply an exhaustion of labile DOC components, resulting in diminished microbial Fe reduction. The latter is confirmed by a lower release of Fe_{aq}—most of which was Fe(II)—at later stages of soil reduction, especially in the straw-amended soils (Fig. 3). The increasing Fe_{aq} concentrations at the end of the first three reduction cycles (42 days) of the 14-day cycle experiment agree well with increasing Fe(II) concentrations extracted by 0.5 M HCl in the 14-day cycle soil incubation experiment (56 days) of Ginn et al. (2017), which they ascribed to the neo-formation of a 'rapidly reducible' Fe(III) pool. Our observation also accords with Winkler et al. (2018) who showed an initially increasing (up to 168 days) and then declining $Fe(II)_{aq}$ release for an Andosol dominated by SRO Fe(III) phases, which was redox-cycled with straw addition for one year with periods of 5 weeks spent under anoxic and one week under oxic conditions. Decreasing Fe_{aq} releases in our high-OC treatments (after 42 days in the 14-day cycle experiment) (Fig. 3) indicate that 'rapidly reducible' Fe(III) did not accumulate under conditions of low redox frequency and during prolonged redox cycling at high redox frequency. Instead, plateauing Fe_{aq} concentrations in the 28-day cycle, high-OC experiment (Fig. 3) suggest that the pool of reducible Fe was depleted earlier after each reduction–oxidation cycle. We propose several explanations for the decreasing maximum Fe_{aq} concentrations in the high-OC treatments, particularly in the 28-day cycle experiment: Dissolved Fe(II) was physically removed at the end of each reduction period in our experiments via leaching and could thus not precipitate as rapidly reducible SRO Fe(III) solids upon soil re-oxidation for the most part (Barcellos et al., 2018; Ginn et al., 2017). Preferential dissolution of the least ordered Fe oxides during initial reduction cycles, supported by initially higher concentrations of labile straw DOC components, led to an enhanced crystallinity of residual soil Fe oxides (see next paragraphs) and thus diminished the extent of Fe reduction with increasing redox fluctuation time. In addition, the OC and Si loading of residual SRO Fe(III) solids may have progressively increased with each new redox cycle in the high-OC treatments owing to increasing DOC and Si concentrations during reduction periods (Figs. 3 and S15). Therefore, blockage of Fe(III) sites by sorbed OM and/or Si may have stabilized SRO Fe(III) solids against bioreduction (Chen et al., 2015; Eusterhues et al., 2014; Jones et al., 2009; Shimizu et al., 2013; Zhou et al., 2018). Finally, because we added straw as an electron donor at the beginning of our experiments—a scenario more typical of arable floodplain soils subjected to phreatic rather than fluvial flooding (Kirk, 2004)—this may have caused organic substrate or nutrient (e.g., P) limitation for Fe(III) reducers (Chacon et al., 2006; Ginn et al., 2017; Parsons et al., 2013) at later stages of our experiments. Because we observed significantly higher losses of OC and Fe at higher redox frequency in straw-amended soils (Fig. 6), our results suggest generally higher OC and metal(loid) losses from OM-rich soils exposed to more frequent redox changes as compared to those with less frequent redox changes.

4.2. Effect of organic matter on solid-phase Fe speciation

The initial Fe speciation in our soil was dominated by ferrihydrite and vSRO Fe(III) solids, whereas more crystalline Fe oxides (lepidocrocite and hematite) and Fe-bearing phyllosilicates were of lower abundance (Tables 2 and 3). Therefore, the evolution of Fe speciation in our study was mainly governed by pre-existing SRO Fe(III) solids and OM. Leaching conditions had a negligible impact on total soil Fe losses in the low-OC treatments (0.5–1.6 %), but accounted for up to 4.4 % of Fe_{tot} in the high-OC treatments (Fig. 6, Table 1). Therefore, Fe speciation changes > 5 % observed in our study largely reflect in-situ changes.

Compared to the controls, we recorded an absolute mean decline of SRO Fe oxides (Fe_o–Fe_p) of up to 19 % in straw-amended soils after

Table 3
Spectral areas (%) of Fe components in 5-K ^{57}Fe Mössbauer spectra and derived crystallinity index of distinct Fe oxides (ferrihydrite, lepidocrocite, and hematite) for the original soil and re-oxidized soil samples of the 14- and 28-day cycle experiments.[a]

f_{redox} (days/cycle)	Cycle	Q-Fe(III)	Q/H-Fe(II)[b]	H-OxHy	H-(b)OxHy	H-Ox	Crystallinity index[c]
			Original soil				
0	0	15	13	37	24	11	0.65
			0 g/kg OC				
14	4	17	15	32	24	12	0.71
14	8	18	12	34	24	12	0.73
28	2	16	14	31	28	11	0.75
28	4	18	16	31	24	11	0.80
			10 g/kg OC				
14	4	18	14	28	28	12	0.83
14	8	19	15	26	28	12	0.86
28	2	18	16	29	27	11	0.81
28	4	18	15	26	29	12	0.87
			50 g/kg OC				
14	4	19	13	25	31	12	0.92
14	8	22	16	23	28	12	0.96
28	2	18	15	28	28	11	0.85
28	4	19	15	24	31	11	0.95

[a] Area uncertainties (2σ) are in the range of ~ 1 %. Component interpretation: Q-Fe(III) = mononuclear organic Fe(III) complexes and Fe(III) in low-Fe silicates, Q/H-Fe(II) = silicate-bound Fe(II), H-OxHy = Fe(III) oxyhydroxides and ferrihydrite, H-(b)OxHy = Fe(III) species with very short-range order ('vSRO Fe(III) solids'), H-Ox = hematite.
[b] Values include the area of magnetically ordered Fe(II) (H-(b)Fe(II), < 6 %).
[c] Calculated as $\sum$(H-OxHy, H-Ox)$_{77\ K}$ / $\sum$(H-OxHy, H-Ox)$_{5\ K}$.

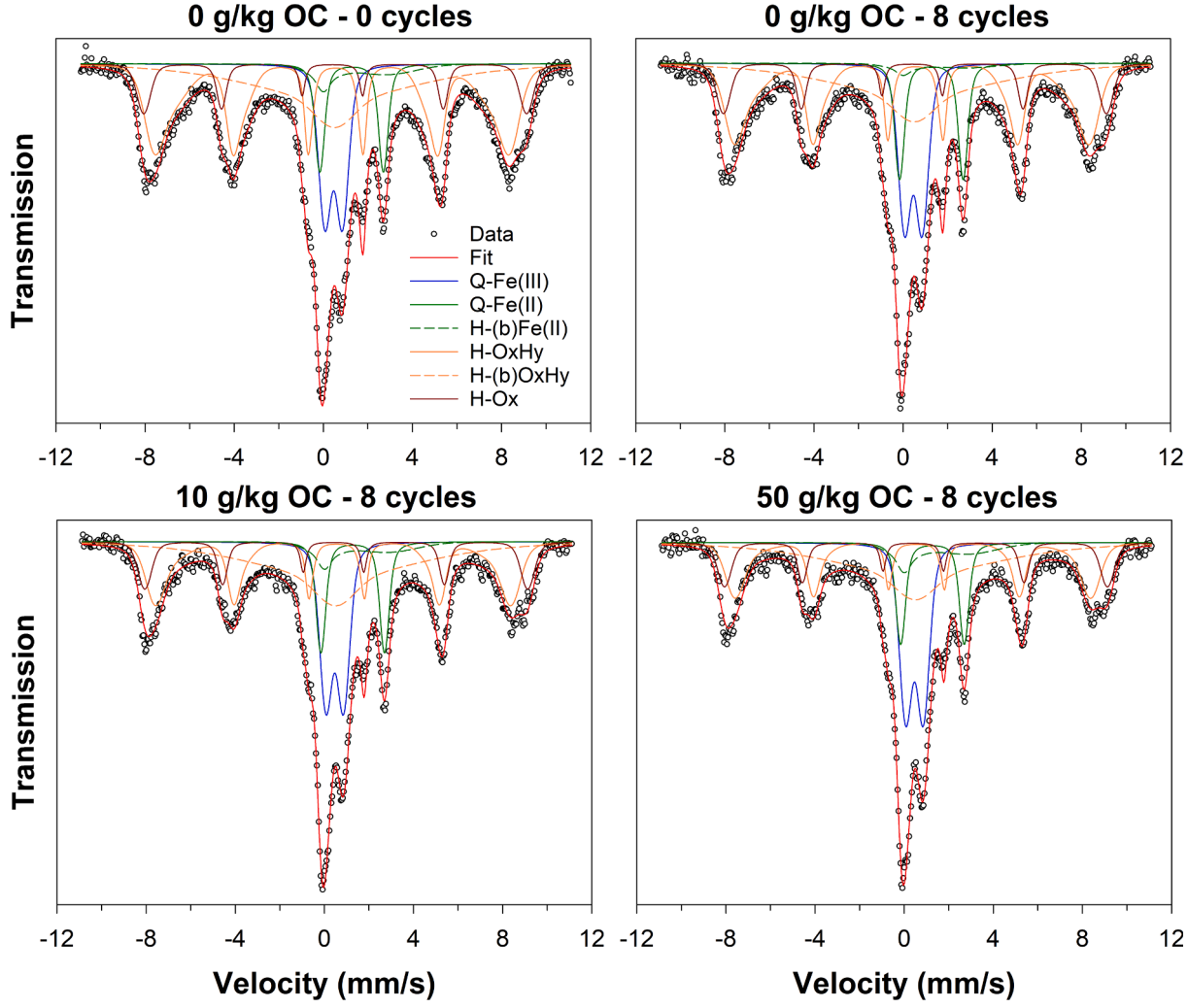

Fig. 10. 5-K ^{57}Fe Mössbauer spectra of soil samples amended with 0, 10, and 50 g/kg straw-OC and subject to eight redox cycles at f_{redox} = 14 days/cycle. Each redox cycle included a reduction and oxidation period of 12 and 2 days, respectively. The spectrum of the original soil is shown for comparison and the legend is valid for all panels. Component interpretation: Q-Fe(III) = mononuclear organic Fe(III) complexes and Fe(III) in low-Fe silicates, Q-Fe(II) and H-(b)Fe(II) = silicate-bound Fe(II), H-OxHy = Fe(III) oxyhydroxides and ferrihydrite, H-(b)OxHy = Fe(III) species with very short-range order ('vSRO Fe(III) solids'), H-Ox = hematite. Fit results are presented in Tables 3 and S7. Additional spectra are shown in Figures S3-14.

112 days of redox cycling, illustrating that straw additions stimulated the bioreduction of ferrihydrite during anoxic periods, perhaps enhanced by associated OM (Cooper et al., 2017) and ligand-promoted dissolution owing to high DOC concentrations (Fig. 3). Likewise, decreases in the mean $(Fe_o–Fe_p)/Fe_{tot}$ ratio up to 20 % relative to the controls and concomitant decreases in the mean Fe_o/Fe_d ratio up to 10 % relative to the controls document that high straw additions led to a relative depletion of ferrihydrite and a relative enrichment of more crystalline Fe oxides upon soil redox cycling for 112 days. The increased crystallinity of Fe oxides was most likely caused by a combination of preferential microbial reductive dissolution of the least ordered ferrihydrites during anoxic periods (Li et al., 2012; Mansfeldt et al., 2012; Poggenburg et al., 2018; Zhang et al., 2020), Fe(II)-catalyzed Fe-oxide recrystallization (Hansel et al., 2003; Pedersen et al., 2005), preferential ligand-promoted dissolution of ferrihydrite over more crystalline Fe oxides (Nowack and Sigg, 1997; Stumm et al., 1985), and reprecipitation of more crystalline (SRO) Fe oxides during soil oxidation through templating (Chen and Thompson, 2021; Larese-Casanova et al., 2012). However, the fact that the crystallinity index of distinct Fe oxides in the control treatments increased in a similar manner as in the high-OC treatments despite negligible Fe losses (Table 3) implies that the increase in Fe-oxide crystallinity in the straw treatments was not primarily influenced by soil Fe losses, but can be largely attributed to in-situ transformation processes.

Our XAS results (f_{redox} = 14 days/cycle) showed that Fe(II) released upon soil reduction and re-sorbed to the soil was efficiently oxidized during oxic periods and therefore did not detectably accumulate in the solid phase. XAS data also demonstrated that straw amendments resulted in mean enrichments of organically complexed Fe(III) of up to 28 % relative to the control and minor mean depletions of Fe oxides, particularly ferrihydrite (<10 % relative to the control). Negative correlations between Fe(III)-citrate and ferrihydrite fractions determined by XAS (r_p = -0.89, $p < 0.0001$, N = 25) and between Fe_p/Fe_{tot} and $(Fe_o–Fe_p)/Fe_{tot}$ (r_p = -0.89, $p < 0.0001$, N = 25) suggest reductively dissolved ferrihydrite partially reprecipitated as organically complexed Fe(III) solids.

Mössbauer spectroscopy revealed that the highest straw levels resulted in a decline of distinct Fe oxides (predominantly ferrihydrite, lepidocrocite, and hematite) by up to 25 % after 112 days when compared to the redox-cycled controls (Table 3). This implies that high OC levels promoted the reductive dissolution of ferrihydrite. The crystallinity of distinct Fe oxides increased markedly in the high-OC treatments, as shown by an up to 31 % increase in their crystallinity index relative to the redox-cycled controls (Table 3). The relative enrichment of more crystalline distinct Fe oxides in straw-amended soil was accompanied by an increase in vSRO Fe(III) solids, whose proportions increased relative to the redox-cycled controls by up to 29 % (Table 3). However, this did not cause an increased Fe release during prolonged soil redox cycling (Fig. 4), suggesting either OC or nutrient limitations, or that OM and Si stabilized these Fe(III) species against bioreduction (Eusterhues et al., 2014; Shimizu et al., 2013). Evidence for substantial Fe(II)-catalyzed transformation of ferrihydrite into thermodynamically more stable Fe oxides like goethite or lepidocrocite, even in presence of abundant OM (Chen et al., 2015), was not observed by XAS and MBS. Rather, our results show that redox oscillations in soil initially dominated by ferrihydrite led to a consortium of increasingly ordered ferrihydrite and vSRO Fe(III) solids.

Our finding of increased Fe-oxide crystallinity is consistent with the increased recrystallization of SRO Fe oxides during soil redox cycling in closed redox-stat reactors observed by Thompson and co-workers (2006). It also agrees with field and laboratory results of Winkler et al. (2018) showing an accumulation of more crystalline Fe oxides for paddy and non-paddy soils initially enriched in SRO Fe oxides. In this study, the increase in Fe-oxide crystallinity was attributed to preferential reduction of SRO Fe oxides coupled to stronger leaching of $Fe(II)_{aq}$ and Fe(II)-catalyzed recrystallization of SRO Fe oxides. The absence of ferrihydrite transformation into crystalline Fe-oxide phases in our experiments suggests that even in the control treatments ferrihydrite was effectively stabilized by sorbed OM and/or Si, which inhibited Fe(II)-catalyzed transformation reactions (Chen et al., 2015; Jones et al., 2009; Zhou et al., 2018). This conclusion is supported by field observations of Vogelsang et al., (2016a) documenting that ferrihydrite exposed to marshland-derived paddy subsoils for 12 months only accumulated a small amount of OC (8 g/kg) due to high pH (>7.0) and salinity, and thus transformed into crystalline Fe oxides (goethite, hematite, and lepidocrocite) instead of vSRO Fe(III) solids. Sorption of DOC and/or Si to resident crystalline Fe and Al oxides may have additionally limited their ability to catalyze the formation of crystalline Fe oxides viz. heterogeneous $Fe(II)_{aq}$ oxidation by O_2 during soil re-oxidization (Chen and Thompson, 2018). Likewise, high DOC concentrations in combination with high bicarbonate concentrations may have prevented lepidocrocite formation, as observed for homogeneous $Fe(II)_{aq}$ oxidation (Chen and Thompson, 2021, 2018), and caused the relative enrichment of vSRO Fe(III) solids in the high-OC treatments.

Based on our results, bulk soils or soil microsites enriched in SRO Fe oxides and subject to frequent and prolonged water saturation over years with ample electron donor supply are likely to lose high-surface area SRO Fe oxides that stabilize soil OC against microbial degradation (Jones and Edwards, 1998; Mikutta et al., 2006; Torn et al., 1997). However, their depletion may be accompanied by the formation of vSRO Fe(III) solids, whose contribution to OC stabilization in redox-active soils is still unclear.

4.3. Effect of redox frequency and time on solid-phase Fe speciation

We observed significant effects of redox frequency and time on soil Fe transformations. Selective Fe extraction data of the low-OC treatments showed that the 28-day cycle experiment resulted in higher absolute and relative contents of crystalline Fe oxides and lower Fe_o/Fe_d ratios (Fig. 7, Table S2). These findings imply that longer reduction–oxidation periods in low-OC soils facilitate Fe-oxide recrystallization, likely due to extended anoxia with more limited sorption competition between DOC (or Si) and $Fe(II)_{aq}$ during anoxic periods. The potentially high DOC (Si)–$Fe(II)_{aq}$ competition in the high-straw treatments explains why redox frequency had no measurable effect on any extractable Fe parameter (Fig. 7, Table S2).

Mössbauer spectroscopy revealed that the highest straw level in the 14-day cycle experiment resulted in a 25 % lower fraction of distinct Fe oxides (primarily ferrihydrite, lepidocrocite, and hematite) after 112 days when compared to the redox-cycled control, whereas this decline was 16 % in the 28-day cycle experiment (Table 3). This suggests that faster redox changes at high OC levels promoted the reductive dissolution of ferrihydrite. The increase in crystallinity of distinct Fe oxides in the high-OC treatments after 112 days was more pronounced in the 14-day cycle compared to the 28-day cycle experiment, as evidenced by a 31 vs. 18 % increase in their crystallinity index relative to the respective controls (Table 3). This difference, however, was only caused by the higher crystallinity index of the straw-free control in the 28-day compared to the 14-day cycle experiment. For the straw-amended soils, MBS revealed no effect of redox frequency on the crystallinity of distinct Fe oxides after 112 days (Table 3), in agreement with selective Fe extraction results (Fig. 7). These results suggest that longer reduction periods in straw-free soil promoted the dissolution of the least ordered ferrihydrites and/or Fe(II)-catalyzed ferrihydrite recrystallization, leading to an enhanced crystallinity of residual (SRO) Fe oxides, whereas high straw additions effectively masked the effect of redox frequency, likely due to a similarly effective microbial utilization of (SRO) Fe oxides as terminal electron acceptors at both redox frequencies.

The proportions of vSRO Fe(III) solids increased by up to 14 % in the 14-day cycle and by 29 % in the 28-day cycle experiment relative to the redox-cycled controls (Table 3), documenting a more pronounced enrichment of vSRO Fe(III) solids at lower redox frequency.

Summarized, MBS revealed a greater relative depletion of distinct Fe oxides (notably ferrihydrite) in straw-amended soils in the 14-day cycle than in the 28-day cycle experiment after 112 days, which was accompanied by a less pronounced relative enrichment of vSRO Fe(III) solids. In addition, MBS showed that the lower redox frequency only enhanced the crystallinity of distinct Fe oxides in the straw-free soil, whereas redox frequency had no effect on the crystallinity of distinct Fe oxides in straw amended soils.

The effect of redox fluctuation time on soil Fe pools was investigated using selective extractions, XAS (at $f_{redox} = 14$ days/cycle), and MBS. Selective Fe extractions essentially showed that prolonged redox cycling under leaching conditions resulted in minor absolute and relative losses of (SRO) Fe oxides (Table S3). These results are supported by XAS showing that straw amendments led to a slightly lower Fe-oxide fraction over time (Table S6), which was also observed for paddy topsoils under prolonged paddy management (Vogelsang et al., 2016b). Mössbauer spectroscopy further showed that prolonged redox cycling of soil increased the crystallinity of distinct Fe oxides in all treatments, which was enhanced by straw additions. Collectively, our results indicate that prolonged and slow redox cycling in high-OM soils dominated by SRO Fe (III) solids leads to a relative enrichment of more crystalline (SRO) Fe oxides and vSRO Fe(III) solids. The formation of the latter Fe species, however, did not translate into an increased reductive Fe_{aq} release (Figs. 3 and 4). This may be explained by three scenarios: (1) the reductive dissolution of vSRO Fe(III) solids during redox cycling was limited by OC or nutrient availability, (2) these solids were effectively stabilized against reductive dissolution by associated OM (or Si), and/or (3) their preferential microbial dissolution (Barcellos et al., 2018; Ginn et al., 2017) was not apparent due to a disproportionate reductive loss of ferrihydrite.

5. Summary and implications

We conducted long-term redox oscillation experiments under leaching conditions at $f_{redox} = 14$ and 28 days/cycle with soil whose initial Fe speciation was dominated by ferrihydrite and vSRO Fe(III) solids likely consisting of polynuclear organic Fe(III) complexes. Our main findings can be summarized as follows:

(1) Iron dissolution and transformation reactions varied with OM content, redox frequency, and redox fluctuation time. Straw additions strongly increased the extent of Fe(III) reduction and DOC release during anoxia. Reduction-induced losses of DOC and Fe_{aq} from straw-amended soils due to leaching prior to soil oxidation were enhanced at high redox frequency.
(2) Despite short re-oxidation times of only 2 or 4 days, Fe(II) did not detectably accumulate in the solid phase of re-oxidized soils. Although Fe(III)-poor phyllosilicates gained in relative importance in all redox treatments compared to the original soil, their fraction was hardly affected by OM content, redox frequency, and redox fluctuation time.
(3) Pre-existing SRO Fe(III) solids and straw-OM were the major determinants of solid-phase Fe speciation changes. High straw additions led to a depletion of ferrihydrite and a relative enrichment of organically complexed Fe(III) during soil redox cycling. Thus, our hypothesis stating that increasing OM levels promote the accumulation of SRO Fe oxides during soil redox cycling must be rejected. The crystallinity of residual distinct Fe oxides—mainly ferrihydrite in addition to lepidocrocite and hematite—increased during soil redox cycling and was enhanced by straw additions. A substantial Fe(II)-catalyzed ferrihydrite transformation into crystalline Fe oxides (goethite and lepidocrocite) could not be detected.
(4) Although organically complexed Fe(III) gained in relative importance during soil redox cycling, particularly in high-OC treatments, this did not lead to an increased Fe release during consecutive reduction events. Soils became progressively less responsive to changes in redox conditions. This was likely caused by removal of reduced solutes from soil, stabilization of Fe(III) by OM and/or Si, and organic substrate or nutrient limitation at later stages of redox fluctuations.
(5) The lower redox frequency enhanced the crystallinity of residual distinct Fe oxides in straw-free soil after 112 days, which is consistent with our hypothesis stating that a lower redox frequency causes more pronounced changes in soil Fe pools. For straw-amended soil, however, redox frequency had no effect on the crystallinity of distinct Fe oxides.
(6) Iron speciation changes became more pronounced with progressive redox fluctuation time, in agreement with our hypothesis. Longer redox cycling resulted in minor losses of (SRO) Fe oxides and a generally increased crystallinity of residual Fe oxides, which was favored by high straw levels and a low redox frequency.

The results obtained in this study can be placed into a broader context because short-term redox fluctuations on a weekly basis are a common feature of natural and anthropogenic soils worldwide. They are common in wetland soils such as marshes, peat bogs, and floodplains, or in soils managed by irrigation farming such as rice paddies. They also occur as a consequence of rainfall events in upland soils, in which zones of transient oxygen depletion (anoxic microsites) are increasingly recognized as an important control of soil OC cycling (Keiluweit et al., 2017, 2016; Lacroix et al., 2022). Our results corroborate that the trajectory of Fe speciation changes in redox-active soils dominated by SRO Fe(III) solids depends crucially on OM content, time of water saturation, and solution conditions (notably pH), as these factors regulate microbial activity, the extent of OM–Fe interactions, and thus the magnitude of bioreduction and transformation of SRO Fe(III) solids. We showed that soil redox oscillations can cause divergent transformations of SRO Fe oxides on comparatively short time scales, leading to an increased crystallinity of residual SRO Fe oxides and the concomitant formation of highly disordered Fe(III) solids. While both processes have previously been documented for soils independently (Ginn et al., 2017; Thompson et al., 2011, 2006; Winkler et al., 2018, 2016), their co-occurrence has—to the best of our knowledge—not yet been reported. Our results imply that Fe(III) mineral transformations in redox-active soils are not strictly unidirectional and may lead to Fe(III) species with contrasting physicochemical properties. This could have implications for other element cycles in redox-active soils and warrants further research on the functional and physicochemical differences between SRO Fe oxides and vSRO Fe(III) solids. Furthermore, our results suggest that faster redox cycling in bulk soils or soil microsites due to weekly redox pulsing leads to higher element exports (e.g., OC and metal(loid)s) from soil than more slowly alternating redox changes under conditions of ample electron donor supply and water leaching. More research is required to explore interdependencies of factors influencing soil Fe pools in redox-active soils, particularly redox frequency, the role of OM quality and recharge patterns, and nutrient availability to soil microorganisms.

Data availability

Data are available through the Research Data Repository of Gottfried Wilhelm Leibniz University Hannover at https://doi.org/10.25835/7ujy6oc0.

CRediT authorship contribution statement

Christian Mikutta: Conceptualization, Formal analysis, Funding acquisition, Investigation, Project administration, Resources, Supervision, Validation, Visualization, Writing – original draft, Writing – review & editing. **Max Niegisch:** Validation, Writing – original draft, Writing – review & editing, Formal analysis, Investigation. **Aaron Thompson:**

Formal analysis, Writing – original draft, Writing – review & editing, Investigation, Resources. **Ricarda Behrens:** Writing – original draft, Writing – review & editing, Investigation. **Laura S. Schnee:** Investigation, Writing – original draft, Writing – review & editing. **Martin Hoppe:** Investigation, Resources, Writing – original draft, Writing – review & editing. **Reiner Dohrmann:** Formal analysis, Investigation, Project administration, Resources, Supervision, Writing – original draft, Writing – review & editing.

Declaration of competing interest

The authors declare that they have no known competing financial interests or personal relationships that could have appeared to influence the work reported in this paper.

Acknowledgements

We thank the ELETTRA synchrotron facility (Trieste, Italy) for the provision of beamtime and Luca Olivi for his excellent support at beamline 11.1. We are grateful to Robert Mikutta for providing the rice straw and to Astrid Jaeckel and Christiane Kamphuis for performing the Fe_o and Fe_d extractions. This work was financially supported by the German Research Foundation, DFG (project no. 418449917).

Appendix A. Supplementary material

The supplementary material contains statistical test results for selective Fe extraction and Fe EXAFS data, results of Fe XANES, EXAFS, and Mössbauer spectroscopy analyses, and information on dissolved Si concentrations.

Supplementary material to this article can be found online at https://doi.org/10.1016/j.gca.2024.02.009.

References

Abdelmoula, M., Trolard, F., Bourrié, G., Génin, J.-M.-R., 1998. Evidence for the Fe(II)-Fe (III) green rust "Fougerite" mineral occurrence in a hydromorphic soil and its transformation with depth. Hyperfine Interact. 112, 235–238.

Barcellos, D., O'connell, C.S., Silver, W., Meile, C., Thompson, A., 2018. Hot spots and hot moments of soil moisture explain fluctuations in iron and carbon cycling in a humid tropical forest soil. Soil Syst. 2, 1–22.

Bhattacharyya, A., Campbell, A.N., Tfaily, M.M., Lin, Y., Kukkadapu, R.K., Silver, W.L., Nico, P.S., Pett-Ridge, J., 2018. Redox fluctuations control the coupled cycling of iron and carbon in tropical forest soils. Environ. Sci. Technol. 52, 14129–14139.

Blowes, D.W., Ptacek, C.J., Jambor, J.L., Weisener, C.G., 2003. The geochemistry of acid mine drainage. In: Turekian, K.K. (Ed.), Treatise on Geochemistry. Pergamon, Oxford, pp. 149–204.

Brandt, O., 2003. Eintrags- und Wirkungspfade von Schwermetallen und Arsen in Flußaue-Systemen am Beispiel der Mulde zwischen Bitterfeld/Wolfen und Dessau, Sachsen-Anhalt (PhD thesis). Technische Universität Berlin, Berlin, Germany.

Braunschweig, J., Klier, C., Schröder, C., Händel, M., Bosch, J., Totsche, K.U., Meckenstock, R.U., 2014. Citrate influences microbial Fe hydroxide reduction via a dissolution-disaggregation mechanism. Geochim. Cosmochim. Acta 139, 434–446.

Buettner, S.W., Kramer, M.G., Chadwick, O.A., Thompson, A., 2014. Mobilization of colloidal carbon during iron reduction in basaltic soils. Geoderma 221–222, 139–145.

Burton, E.D., Bush, R.T., Johnston, S.G., Sullivan, L.A., Keene, A.F., 2011. Sulfur biogeochemical cycling and novel Fe-S mineralization pathways in a tidally re-flooded wetland. Geochim. Cosmochim. Acta 75, 3434–3451.

Chacon, N., Silver, W.L., Dubinsky, E.A., Cusack, D.F., 2006. Iron reduction and soil phosphorus solubilization in humid tropical forests soils: The roles of labile carbon pools and an electron shuttle compound. Biogeochemistry 78, 67–84.

Chen, C., Thompson, A., 2018. Ferrous iron oxidation under varying pO2 levels: The effect of Fe(III)/Al(III) oxide minerals and organic matter. Environ. Sci. Technol. 52, 597–606.

Chen, C., Barcellos, D., Richter, D.D., Schroeder, P.A., Thompson, A., 2019. Redoximorphic Bt horizons of the Calhoun CZO soils exhibit depth-dependent iron-oxide crystallinity. J. Soils Sediments 19, 785–797.

Chen, C., Hall, S.J., Coward, E., Thompson, A., 2020. Iron-mediated organic matter decomposition in humid soils can counteract protection. Nat. Commun. 11, 2255.

Chen, C., Thompson, A., 2021. The influence of native soil organic matter and minerals on ferrous iron oxidation. Geochim. Cosmochim. Acta 292, 254–270.

Chen, C., Kukkadapu, R., Sparks, D., 2015. Influence of coprecipitated organic matter on Fe2+(aq)-catalyzed transformation of ferrihydrite: Implications for carbon dynamics. Environ. Sci. Technol. 49, 10927–10936.

Chen, C., Meile, C., Wilmoth, J., Barcellos, D., Thompson, A., 2018. Influence of pO_2 on iron redox cycling and anaerobic organic carbon mineralization in a humid tropical forest soil. Environ. Sci. Technol. 52, 7709–7719.

Cooper, R.E., Eusterhues, K., Wegner, C.-E., Totsche, K.U., Küsel, K., 2017. Ferrihydrite-associated organic matter (OM) stimulates reduction by Shewanella oneidensis MR-1 and a complex microbial consortia. Biogeosciences 14, 5171–5188.

Cornell, R.M., Schwertmann, U., 2003. The Iron Oxides. Structure, Properties, Reactions, Occurences and Uses, 2nd ed. Wiley-VCH, Weinheim.

Dannenberg, S., Wudler, J., Conrad, R., 1997. Agitation of anoxic paddy soil slurries affects the performance of the methanogenic microbial community. FEMS Microbiol. Ecol. 22, 257–263.

DIN EN ISO 10390:2022-08, Soil, treated biowaste and sludge - Determination of pH (ISO 10390:2021); German version EN ISO 10390:2022.

DIN EN ISO 11260:2018-11, Soil quality - Determination of effective cation exchange capacity and base saturation level using barium chloride solution (ISO 11260:2018); German version EN ISO 11260:2018.

Duong, T.T.T., Baumann, K., Marschner, P., 2009. Frequent addition of wheat straw residues to soil enhances carbon mineralization rate. Soil Biol. Biochem. 41, 1475–1482.

Eusterhues, K., Rennert, T., Knicker, H., Kögel-Knabner, I., Totsche, K.U., Schwertmann, U., 2011. Fractionation of organic matter due to reaction with ferrihydrite: coprecipitation versus adsorption. Environ. Sci. Technol. 45, 527–533.

Eusterhues, K., Hadrich, A., Neidhardt, J., Kusel, K., Keller, T., Jandt, K., Totsche, K., 2014. Reduction of ferrihydrite with adsorbed and coprecipitated organic matter: microbial reduction by *Geobacter bremensis* vs. abiotic reduction by Na-dithionite. Biogeosciences 11, 4953–4966.

Fredrickson, J.K., Zachara, J.M., Kennedy, D.W., Dong, H., Onstott, T.C., Hinman, N.W., Li, S.-M., 1998. Biogenic iron mineralization accompanying the dissimilatory reduction of hydrous ferric oxide by a groundwater bacterium. Geochim. Cosmochim. Acta 62, 3239–3257.

Giannetta, B., Plaza, C., Thompson, A., Plante, A.F., Zaccone, C., 2022. Iron speciation in soil size fractions under different land uses. Geoderma 418, 115842.

Gillman, G.P., 1979. A proposed method for the measurement of exchange properties of highly weathered soils. Aust. J. Soil Res. 17, 129–139.

Ginn, B., Meile, C., Wilmoth, J., Tang, Y., Thompson, A., 2017. Rapid iron reduction rates are stimulated by high-amplitude redox fluctuations in a tropical forest soil. Environ. Sci. Technol. 51, 3250–3259.

Grybos, M., Davranche, M., Gruau, G., Petitjean, P., Pédrot, M., 2009. Increasing pH drives organic matter solubilization from wetland soils under reducing conditions. Geoderma 154, 13–19.

Hansel, C.M., Benner, S.G., Neiss, J., Dohnalkova, A., Kukkadapu, R.K., Fendorf, S., 2003. Secondary mineralization pathways induced by dissimilatory iron reduction of ferrihydrite under advective flow. Geochim. Cosmochim. Acta 67, 2977–2992.

Hendershot, W.H., Lalande, H., Duquette, M., 2008a. Ion exchange and exchangeable cations. In: Carter, M.R., Gregorich, E.G. (Eds.), Soil Sampling and Methods of Analysis. Canadian Society of Soil Science and CRC Press, Boca Raton, FL, USA, pp. 197–206.

Hendershot, W.H., Lalande, H., Duquette, M., 2008b. Soil reaction and exchangeable acidity. In: Carter, M.R., Gregorich, E.G. (Eds.), Soil Sampling and Methods of Analysis. Canadian Society of Soil Science and CRC Press, Boca Raton, FL, USA, pp. 173–178.

Hiemstra, T., 2013. Surface and mineral structure of ferrihydrite. Geochim. Cosmochim. Acta 105, 316–325.

Hoffmann, M., Mikutta, C., Kretzschmar, R., 2013. Arsenite binding to natural organic matter: spectroscopic evidence for ligand exchange and ternary complex formation. Environ. Sci. Technol. 47, 12165–12173.

Huang, X., Kang, W., Wang, L., Yu, G., Ran, W., Hong, J., Shen, Q., 2020. Preservation of organic carbon promoted by iron redox transformation in a rice-wheat cropping system. Appl. Soil Ecol. 147, 103425.

ISO 11277:2020-04, Soil quality - Determination of particle size distribution in mineral soil material - Method by sieving and sedimentation.

Jones, A., Collins, R., Rose, J., Waite, T., 2009. The effect of silica and natural organic matter on the Fe(II)-catalysed transformation and reactivity of Fe(III) minerals. Geochim Cosmochim Acta 73, 4409–4422.

Jones, D.L., Edwards, A.C., 1998. Influence of sorption on the biological utilization of two simple carbon substrates. Soil Biol. Biochem. 30, 1895–1902.

Kaden, U.S., Fuchs, E., Geyer, S., Hein, T., Horchler, P., Rupp, H., Scholz, M., Schulz-Zunkel, C., Weigelhofer, G., 2021. Soil characteristics and hydromorphological patterns control denitrification at the floodplain scale. Front. Earth Sci. 9, 708707.

Keiluweit, M., Nico, P.S., Kleber, M., Fendorf, S., 2016. Are oxygen limitations under recognized regulators of organic carbon turnover in upland soils? Biogeochemistry 127, 157–171.

Keiluweit, M., Wanzek, T., Kleber, M., Nico, P., Fendorf, S., 2017. Anaerobic microsites have an unaccounted role in soil carbon stabilization. Nat. Commun. 8, 1771.

Kirk, G., 2004. The Biogeochemistry of Submerged Soils. John Wiley & Sons Ltd, Chichester, England.

Lacroix, E.M., Mendillo, J., Gomes, A., Dekas, A., Fendorf, S., 2022. Contributions of anoxic microsites to soil carbon protection across soil textures. Geoderma 425, 116050.

Lacroix, E.M., Aeppli, M., Boye, K., Brodie, E., Fendorf, S., Keiluweit, M., Naughton, H.R., Noël, V., Sihi, D., 2023. Consider the anoxic microsite: Acknowledging and appreciating spatiotemporal redox heterogeneity in soils and sediments. ACS Earth Space Chem. 7, 1592–1609.

Langner, P., Mikutta, C., Kretzschmar, R., 2012. Arsenic sequestration by organic sulphur in peat. Nat. Geosci. 5, 66–73.

Larese-Casanova, P., Kappler, A., Haderlein, S.B., 2012. Heterogeneous oxidation of Fe (II) on iron oxides in aqueous systems: Identification and controls of Fe(III) product formation. Geochim. Cosmochim. Acta 91, 171–186.
Li, X., Liu, T., Li, F., Zhang, W., Zhou, S., Li, Y., 2012. Reduction of structural Fe(III) in oxyhydroxides by Shewanella decolorationis S12 and characterization of the surface properties of iron minerals. J. Soils Sediments 12, 217–227.
Maher, B.A., Taylor, R.M., 1988. Formation of ultrafine-grained magnetite in soils. Nature 336, 368–370.
Mansfeldt, T., Schuth, S., Häusler, W., Wagner, F.E., Kaufhold, S., Overesch, M., 2012. Iron oxide mineralogy and stable iron isotope composition in a Gleysol with petrogleyic properties. J. Soils Sediments 12, 97–114.
McKeague, J.A., Brydon, J.E., Miles, N.M., 1971. Differentiation of forms of extractable iron and aluminum in soils. Soil Sci. Soc. Amer. Proc. 35, 33–38.
Mehra, O.P., Jackson, M.L., 1958. Iron oxide removal from soils and clays by a dithionite-citrate system buffered with sodium bicarbonate. Clays Clay Miner. 7, 317–327.
Mejia, J., Roden, E.E., Ginder-Vogel, M., 2016. Influence of oxygen and nitrate on Fe (hydr)oxide mineral transformation and soil microbial communities during redox cycling. Environ. Sci. Technol. 50, 3580–3588.
Mikutta, C., 2011. X-ray absorption spectroscopy study on the effect of hydroxybenzoic acids on the formation and structure of ferrihydrite. Geochim Cosmochim Acta 75, 5122–5139.
Mikutta, R., Kleber, M., Torn, M.S., Jahn, R., 2006. Stabilization of soil organic matter: association with minerals or chemical recalcitrance? Biogeochemistry 77, 25–56.
Mikutta, C., Kretzschmar, R., 2011. Spectroscopic evidence for ternary complex formation between arsenate and ferric iron complexes of humic substances. Environ. Sci. Technol. 45, 9550–9557.
Mikutta, C., Rothwell, J.J., 2016. Peat bogs as hotspots for organoarsenical formation and persistence. Environ. Sci. Technol. 50, 4314–4323.
Nowack, B., Sigg, L., 1997. Dissolution of Fe(III) (hydr)oxides by metal-EDTA complexes. Geochim. Cosmochim. Acta 61, 951–963.
Parsons, C.T., Couture, R.-M., Omoregie, E.O., Bardelli, F., Greneche, J.-M., Roman-Ross, G., Charlet, L., 2013. The impact of oscillating redox conditions: Arsenic immobilisation in contaminated calcareous floodplain soils. Environ. Pollut. 178, 254–263.
Pedersen, H.D., Postma, D., Jakobsen, R., Larsen, O., 2005. Fast transformation of iron oxyhydroxides by the catalytic action of aqueous Fe(II). Geochim. Cosmochim. Acta 69, 3967–3977.
Pei, J., Li, H., Li, S., An, T., Farmer, J., Fu, S., Wang, J., 2015. Dynamics of maize carbon contribution to soil organic carbon in association with soil type and fertility level. PLoS ONE 10, 0120825.
Piepenbrock, A., Dippon, U., Porsch, K., Appel, E., Kappler, A., 2011. Dependence of microbial magnetite formation on humic substance and ferrihydrite concentrations. Geochim. Cosmochim. Acta 75, 6844–6858.
Poggenburg, C., Mikutta, R., Schippers, A., Dohrmann, R., Guggenberger, G., 2018. Impact of natural organic matter coatings on the microbial reduction of iron oxides. Geochim. Cosmochim. Acta 224, 223–248.
Rancourt, D.G., Ping, J.Y., 1991. Voigt-based methods for arbitrary-shape static hyperfine parameter distributions in Mössbauer spectroscopy. Nucl. Instrum. Methods Phys. Res. B 58, 85–97.
Ravel, B., Newville, M., 2005. ATHENA, ARTEMIS, HEPHAESTUS: data analysis for X-ray absorption spectroscopy using IFEFFIT. J Synchrotron Rad 12, 537–541.
Reddy, K.R., DeLaune, R.D., 2008. Biogeochemistry of Wetlands: Science and Applications, 1st ed. CRC Press, Boca Raton, FL.
Rennert, T., 2019. Wet-chemical extractions to characterise pedogenic Al and Fe species - a critical review. Soil Res. 57, 1–16.
Rolf, M., Laermanns, H., Kienzler, L., Pohl, C., Möller, J.N., Laforsch, C., Löder, M.G.J., Bogner, C., 2022. Flooding frequency and floodplain topography determine abundance of microplastics in an alluvial Rhine soil. Sci. Total Environ. 836, 155141.
Scheinost, A.C., Kretzschmar, R., Pfister, S., Roberts, D.R., 2002. Combining selective sequential extractions, X-ray absorption spectroscopy, and principal component analysis for quantitative zinc speciation in soil. Environ. Sci. Technol. 36, 5021–5028.
Schwertmann, U., 1964. Differenzierung der Eisenoxide des Bodens durch Extraktion mit Ammoniumoxalat-Lösung. Z. Pflanzenernähr. Düng. Bodenk. 105, 194–202.
Shimizu, M., Zhou, J., Schröder, C., Obst, M., Kappler, A., Borch, T., 2013. Dissimilatory reduction and transformation of ferrihydrite-humic acid coprecipitates. Environ. Sci. Technol. 47, 13375–13384.
Stookey, L.L., 1970. Ferrozine-a new spectrophotometric reagent for iron. Anal. Chem. 42, 779–781.
Stumm, W., Furrer, G., Wieland, E., Zinder, B., 1985. The effects of complex-forming ligands on the dissolution of oxides and aluminosilicates. In: Drever, J.I. (Ed.), The Chemistry of Weathering. D. Reidel, Dordrecht, The Netherlands, pp. 55–74.
Su, Y., He, Z., Yang, Y., Jia, S., Yu, M., Chen, X., Shen, A., 2020. Linking soil microbial community dynamics to straw-carbon distribution in soil organic carbon. Sci. Rep. 10, 5526.
Thompson, A., Chadwick, O.A., Rancourt, D.G., Chorover, J., 2006. Iron-oxide crystallinity increases during soil redox oscillations. Geochim. Cosmochim. Acta 70, 1710–1727.
Thompson, A., Rancourt, D.G., Chadwick, O.A., Chorover, J., 2011. Iron solid-phase differentiation along a redox gradient in basaltic soils. Geochim. Cosmochim. Acta 75, 119–133.
Tomaszewski, E.J., Cronk, S.S., Gorski, C.A., Ginder-Vogel, M., 2016. The role of dissolved Fe(II) concentration in the mineralogical evolution of Fe (hydr)oxides during redox cycling. Chem. Geol. 438, 163–170.
Torn, M.S., Trumbore, S.E., Chadwick, O.A., Vitousek, P.M., Hendricks, D.M., 1997. Mineral control of soil organic carbon storage and turnover. Nature 389, 170–173.
Trolard, F., Génin, J.-M.-R., Abdelmoula, M., Bourrié, G., Humbert, B., Herbillon, A., 1997. Identification of a green rust mineral in a reductomorphic soil by Mössbauer and Raman spectroscopies. Geochim. Cosmochim. Acta 61, 1107–1111.
Vandenberghe, R., Hus, J.J., De Grave, E., 1998. Evidence from Mössbauer spectroscopy of neo-formation of magnetite/maghemite in the soils of loess/paleosol sequences in China. Hyperfine Interact. 117, 359–369.
Vogelsang, V., Fiedler, S., Jahn, R., Kaiser, K., 2016a. In-situ transformation of iron-bearing minerals in marshland-derived paddy subsoil. Eur. J. Soil Sci. 67, 676–685.
Vogelsang, V., Kaiser, K., Wagner, F.E., Jahn, R., Fiedler, S., 2016b. Transformation of clay-sized minerals in soils exposed to prolonged regular alternation of redox conditions. Geoderma 278, 40–48.
Winkler, P., Kaiser, K., Kölbl, A., Kühn, T., Schad, P., Urbanski, L., Fiedler, S., Lehndorff, E., Kalbitz, K., Utami, S.R., Cao, Z., Zhang, G., Jahn, R., Kögel-Knabner, I., 2016. Response of Vertisols, Andosols, and Alisols to paddy management. Geoderma 261, 23–35.
Winkler, P., Kaiser, K., Thompson, A., Kalbitz, K., Fiedler, S., Jahn, R., 2018. Contrasting evolution of iron phase composition in soils exposed to redox fluctuations. Geochim. Cosmochim. Acta 235, 89–102.
Zachara, J.M., Kukkadapu, R.K., Fredrickson, J.K., Gorby, Y.A., Smith, S.C., 2002. Biomineralization of poorly crystalline Fe(III) oxides by dissimilatory metal reducing bacteria (DMRB). Geomicrobiol. J. 19, 179–207.
Zhang, F., Battaglia-Brunet, F., Hellal, J., Joulian, C., Gautret, P., Motelica-Heino, M., 2020. Impact of Fe(III) (oxyhydr)oxides mineralogy on iron solubilization and associated microbial communities. Front. Microbiol. 11, 571244.
Zhang, Z., Furman, A., 2021. Soil redox dynamics under dynamic hydrologic regimes - A review. Sci. Total Environ. 763, 143026.
Zhou, Z., Latta, D., Noor, N., Thompson, A., Borch, T., Scherer, M., 2018. Fe(II)-catalyzed transformation of organic matter-ferrihydrite coprecipitates: a closer look using Fe isotopes. Environ. Sci. Technol. 52, 11142–11150.